LNGS - 92/47
November 1992

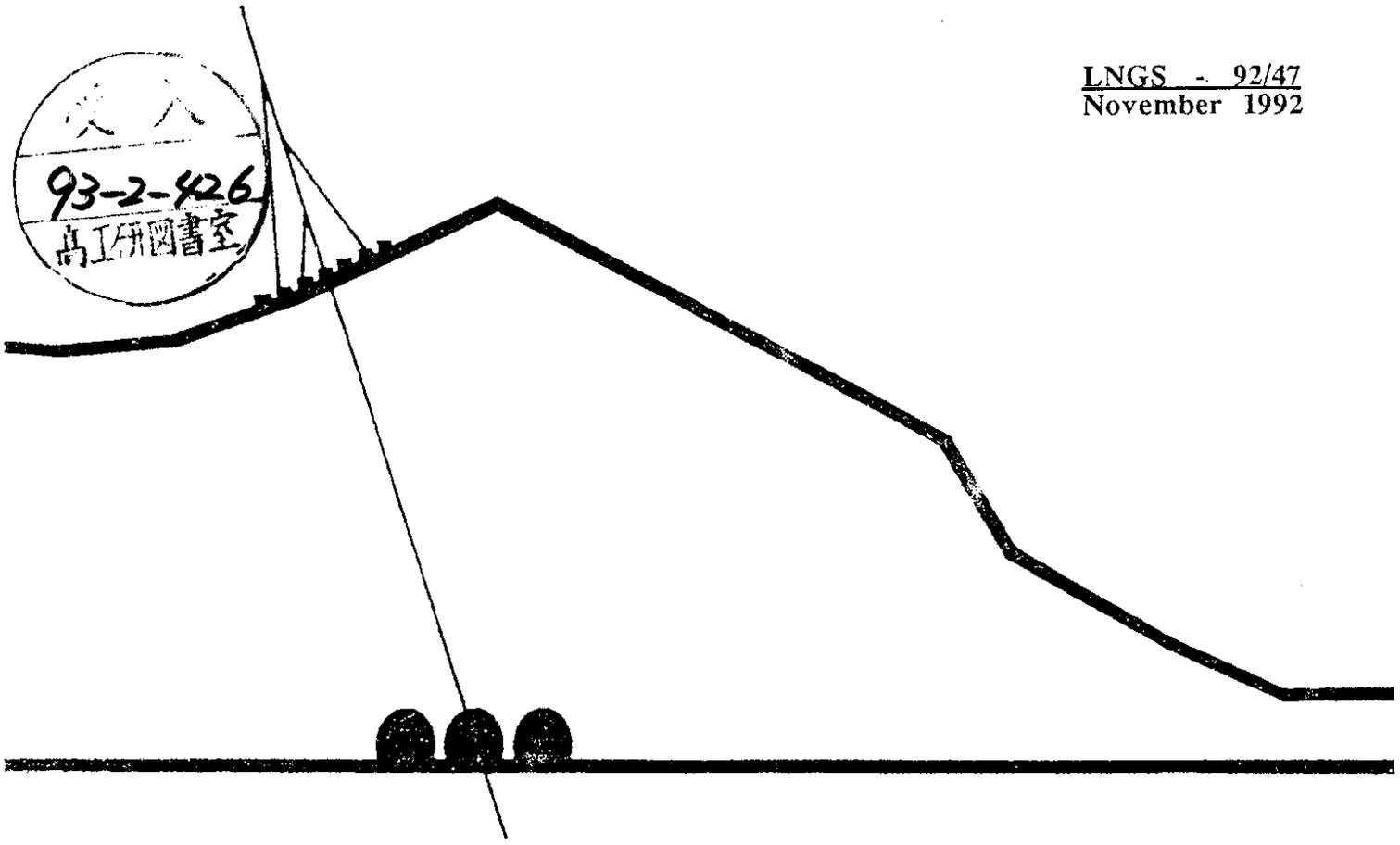

A DETECTOR FOR THE STUDY OF $\overline{\nu}_e e^-$ SCATTERING AT A NUCLEAR REACTOR

The MUNU Collaboration

INFN - Laboratori Nazionali del Gran Sasso

LNGS - 92/47
November 1992

A Detector for the Study of $\overline{\nu}_e e^-$ Scattering at a Nuclear Reactor

MUNU collaboration

C. Broggini
I.N.F.N. Laboratori Nazionali del Gran Sasso, I-67010 Assergi (AQ), Italy

M. Avenier, G. Bagieu, R. Brissot, J.F. Cavaignac, D.H. Koang, D. Lebrun, and A.Stutz
Institut des Sciences Nucléaires, IN2P3-UJF, 53 Avenue des Martyrs, F-38026 Grenoble CEDEX, France

H.W. Becker
Institut für Kernphysik, Wilhelm Klemmstr. 9, D-4400 Münster, Germany

J. Busto, J. Farine, V. Jörgens, A. Tadsen, M. Treichel, and J.-L. Vuilleumier
Institut de Physique, A.-L. Breguet 1, CH-2000 Neuchâtel, Switzerland

D. Gibin, A. Guglielmi, M. Mezzetto, G. Puglierin, and L. Visentin
Dipartimento di Fisica dell'Università and INFN, Via Marzolo 8, I-35100 Padova, Italy

C. Amsler, S. von Dombrowski, E. Holzschuh, and F. Ould-Saada
Physik-Institut, Schönberggasse 9, CH-8001 Zürich, Switzerland

Abstract

We intend to build a low backgroud detector based on a gas TPC to be installed near a nuclear reactor in Bugey for the experimental study of $\overline{\nu}_e e^-$ scattering. The threshold on the electron recoil energy can be set very low, around 500 keV, giving the experiment a good sensitivity to the magnetic moment of the $\overline{\nu}_e$, extending down to $2\text{–}3 \cdot 10^{-11}$ Bohr magnetons.

Other applications of the proposed detector in low energy particle physics are also discussed.

Contents

I. INTRODUCTION, MOTIVATION.

I.1 The physics of neutrinos with magnetic moments and astrophysical implications

The neutrino magnetic moment matrix $\mu_{\ell,\ell'}$ $(\ell, \ell' = e, \mu, \tau)$, like the mass matrix $m_{\ell,\ell'}$, is fundamental and its experimental study may provide insight on new physics.

In the standard model, neutrinos are massless Dirac particles and have vanishing magnetic moments. In the simplest extension neutrinos are still Dirac particles but may have masses and acquire a magnetic moment through radiative corrections [1], [2],

$$\mu_{\ell\ell'} = \frac{3G_F e m_{\ell\ell'}}{8\sqrt{2}\pi^2} = 3.2 \cdot 10^{-19} \cdot m_{\ell\ell'}(eV) \tag{1}$$

in Bohr magneton units, much too small however to be of any significance in lab experiments or in astrophysics. In left-right symmetric models the magnetic moments can be more important, of order 10^{-14} for the ν_e. This is still small for presently planned experiments. But models predicting moments up to 10^{-10} have been built (see for instance [3], [4], [5], [6], [7], [8]). These models incorporate new particles, for instance they have a richer Higgs sector. Neutrinos may be of Dirac or Majorana type, with the restriction, in the Majorana case, that $\mu_{\ell\ell'}$ is antisymmetric and only transition moments connecting different flavors are allowed, but not static moments.

Magnetic moments will give the neutrinos electromagnetic interaction, allowing scattering from the active left handed $\nu_{\ell L}$ states into the sterile $\nu_{\ell' R}$ states. Scattering cross-sections for both neutrino-baryon and neutrino-electron will be affected, which makes it possible to find evidence for magnetic moments in lab experiments. The contribution, compared to that of the usual weak interaction, increases with decreasing neutrino energy [9]. But at low energy the baryon recoil is very small and difficult to measure. The electron recoil energy is much larger and the best way of looking for the magnetic moment of the ν_e seems to be the detailed study of

$$\overline{\nu}_e e^- \rightarrow \overline{\nu}_e e^- \text{ and } \nu_e e^- \rightarrow \nu_e e^- \tag{2}$$

scattering at low energy. More generally these reactions are fundamental and their study provides information on basic features of the weak interaction. Both charged (CC) and neutral currents (NC) are involved. They are expected to interfere if the NC and CC final state neutrinos are identical, as assumed in the standard model [10]. A measurement of the differential cross section of either reaction allows, in principle, to determine the Weinberg angle $sin^2\theta_W$ and to observe the interference which is expected to be destructive for reasonable values of $sin^2\theta_W$. Practically however $\overline{\nu}_e e^- \rightarrow \overline{\nu}_e e^-$ only has a good sensitivity to both effects, while $\nu_e e^- \rightarrow \nu_e e^-$ essentially probes the interference only.

The differential cross section is given by [9], [10]:

$$\frac{d\sigma}{dT} = \frac{G_F^2 m_e}{2\pi}\left[(g_V + x + g_A)^2 + (g_V + x - g_A)^2\left(1 - \frac{T}{E_\nu}\right)^2 + (g_A^2 - (g_V + x)^2)\frac{m_e T}{E_\nu^2}\right] + \frac{\pi\alpha^2\mu_\nu^2}{m_e^2}\frac{1 - T/E_\nu}{T} \tag{3}$$

where T is the electron kinetic recoil energy, E_ν the neutrino energy; in the standard model one has:

$$g_V = 2sin^2\theta_W + \frac{1}{2},\ \ g_A = \begin{cases} \frac{1}{2} & \text{for } \nu_e \\ -\frac{1}{2} & \text{for } \overline{\nu}_e \end{cases}$$

Here

$$\mu_\nu = \sqrt{\sum_\ell |\mu_{e\ell}|^2}$$

is the effective magnetic moment; x is calculated from the neutrino form factors, for Dirac neutrinos it is related to the square charge radius $< r^2 >$ of the neutrino

$$x = \frac{2M_W^2}{3} < r^2 > sin^2\theta_W \text{ for } \nu_e,\ x \to -x \text{ for } \overline{\nu}_e \tag{4}$$

The terms on the first line are due essentially to W and Z exchange. Their contribution to the total cross-section increases linearly with E_ν. The term on the second line comes from the magnetic moment interaction, and its contribution increases only logarithmically. To observe this term one must use low energy neutrinos.

But the most spectacular consequence of magnetic moments will be the precession of neutrinos from left handed $\nu_{\ell L}$ states to right handed $\nu_{\ell' L}$ states in the presence of a transverse magnetic field $\vec{B}_\perp$. In vacuum, assuming for simplification two neutrino states ℓ and ℓ' diagonal in the mass, the evolution is given by:

$$i\frac{d}{dt}\begin{pmatrix} \nu_{\ell L} \\ \nu_{\ell' R} \end{pmatrix} = \begin{pmatrix} -\Delta m^2/4E & \mu_{\ell\ell'}B_\perp \\ \mu_{\ell\ell'}B_\perp & \Delta m^2/4E \end{pmatrix}\begin{pmatrix} \nu_{\ell L} \\ \nu_{\ell' R} \end{pmatrix} \tag{5}$$

Here E is the neutrino energy, and $\Delta m^2 = m_{\ell' R}^2 - m_{\ell L}^2$ is the difference of the squared masses. In case of equal masses, for instance if the neutrinos are Dirac with $\ell = \ell'$, the precession frequency is $|\mu_{\ell\ell'}||B_\perp|$. This is too small to have any effect in terrestrial experiments, but may be important in astrophysical systems.

In fact, solar neutrino astronomy is at the origin of the recent interest in the magnetic moment of the neutrino. Such a moment might be responsible for the observed low flux of ^8B ν_e from the sun in the ^{37}Cl [11] (also see ref. [12]) and Kamiokande experiments [13]. These neutrinos have relatively large energies, several MeV. Voloshin, Vysotskii and Okun [14] have pointed out that the sun, in solar active years, has a nearly toroidal

magnetic field above and below the equator, in the $2 \cdot 10^{10}$ cm deep convective zone. The strength , during solar active years, is of order a few kG. If some μ_{el} is of order $10^{-10} - 10^{-11}$, the ^8B ν_e, which are produced very near the center of the sun, may flip their spin on their way out when crossing the magnetic field, and become sterile. One then expects the solar ^8B flux to be modulated with the 11 year solar cycle, which is in fact suggested by the ^{37}Cl data, although not observed by Kamiokande.

To be precise, in addition to the magnetic moments, a complete treatment of neutrino propagation must take into account the interaction with matter and the effect of masses, diagonal or not [15], [16]. The magnetic field in the core interior may also be important. The field distribution in the sun interior is poorly known, and assumptions must be made. Many scenarios are possible, depending on the choice of parameters [17], [18], [19]. Suppression of the precession, or complete conversion from one state to an other, can then occur. Also, it may be necessary to include three families of fermions in the calculations, instead of two, as is done usually to simplify [20]. Considering all these parameters, it seems possible to reconcile [21], [22] the fluxes and time dependence of the ^{37}Cl and Kamiokande experiments, as well as the flux of low energy neutrinos, below expectations, reported by the ^{71}Ga GALLEX experiment [23], [24].

Astrophysical observations suggest that, with moments of order $10^{-10} - 10^{-11}$, neutrinos would be of the Majorana type. If neutrinos were Dirac particles, then the observed duration (several seconds) of the SN1987A neutrino burst implies much smaller values: $\mu_{\nu\nu'} < 1 - 20 \cdot 10^{-13}$ [25], [26], [27]. These limit assume that right-handed neutrinos are sterile and can escape from the supernova, and in any case do not apply to Majorana neutrinos. Limits from stellar cooling apply to both Dirac and Majorana neutrinos, but are less stringent: $\mu_{\nu\nu'} < 3 \cdot 10^{-12} - 10^{-11}$ [9] [28], [29], [30]. This is not in strong conflict with magnetic moments of the strength considered, in particular if one takes into account the model dependence of the astrophysical calculations.

Turning around the argument, one can say that, should the neutrino have a large magnetic moment, it would play an important role in stellar physics. It therefore appears important to look for the neutrino magnetic monent in a lab experiment.

I.2 Present experimental situation

Beam dumps at intermediate energy accelerators produce ν_e with energies from 0 to 50 MeV. The fluxes are not very high however, and the ν_e are accompanied by equal numbers of ν_μ and $\overline{\nu}_\mu$, which complicates the interpretation of the experimental data. A measurements of $\nu_e e^- \rightarrow \nu_e e^-$ scattering has been performed at the LAMPF beam dump [31]. In spite of a limited statistics the experiment showed that there was no room for a constructive interference, and tentatively confirmed the destructive interference. As expected the experiment did not give a precise value for the Weinberg angle. It also produced a not very stringent upper limit for the magnetic moment of the ν_e: $\mu_\nu < 1.08 \cdot 10^{-9}$ [32].

Nuclear reactors appear more attractive. They are copious sources of $\overline{\nu}_e$ with energies

between 0 and 8 MeV and are ideally suited for such an experiment. The energy spectra are known with good precision, better than 3 % for E_ν between 1.5 and 8 MeV [33], [9]. Figure 1. shows the expected electron recoil spectra at a ^{235}U reactor, using eq. 3 and taking $sin^2\theta_W = 0.226$. The contribution of W and Z exchange is shown, as well as that from a magnetic moment $\mu_\nu = 10^{-10}$. One sees that the lower the electron recoil the better the sensitivity to the magnetic moment.

Only few attempts have been made to measure $\overline{\nu}_e e^-$ scattering. The UC Irvine group led by F. Reines [34] built the first detector dedicated to the study of elastic $\overline{\nu}_e e^- \rightarrow \overline{\nu}_e e^-$ scattering. The detector was operated successfully at the Savannah River Plant (SRP) in the mid-seventies, where the reaction was observed for the first time. The aim was, in these days, to verify the predictions of the standard model. The detector consisted of a 15.9 kg plastic scintillator, coarsely segmented and surrounded by a NaI counter, a Pb shield and a liquid scintillator to veto cosmics. The signature for a good event was given by a single count in one of the elements of the plastic scintillator with nothing in coincidence. The NaI gave a good anti-Compton efficiency allowing an efficient suppression of the γ background. Events from the $\overline{\nu}_e + p \rightarrow e^+ + n$ reaction in the plastic (200 events·day^{-1}!) were efficiently identified by the detection of the annihilation γ rays and/or by the delayed neutron capture signal in the plastic scintillator or in the NaI, and rejected.

The detector was placed at 11.2 m from the core of the reactor operated, at the time, at a power of 1800 $MWth$, so that the neutrino flux was around $1.9{\cdot}10^{13}$ $cm^{-2}s^{-1}$. Since the cross section is small and the signature rather poor it was necessary to reduce the background from natural activities to a minimum by selecting clean materials for all the components.

Events were recorded during 64.6 days reactor on and 60.7 days reactor off. The count rates in two bins of electron recoil energy T were shown in table 1.

In spite of the low singles background the signal to noise ratio is somewhat marginal.

Table 1: Event rate in the Savannah River experiment

$T(MeV)$	Events/day		
	Reactor on	Reactor off	on-off
1.5-3	45.1 ± 1.0	39.2 ± 0.9	5.9 ± 1.4
3-4.5	2.4 ± 0.19	1.2 ± 0.14	1.2 ± 0.25

These data were compared with standard model predictions based on eq. 3 and on the then accepted reactor spectrum, resulting from a calculation [35]. Agreement was found and the value $\sin^2\theta_W = 0.29 \pm 0.05$ was derived. This is consistent with the best value to date obtained by the CHARM II collaboration [36] in $\nu_\mu e^-$ scattering, an other purely leptonic process: $sin^2\theta_W = 0.232 \pm 0.014$.

We now know however that the reactor spectrum used in this original analysis was much too hard. Vogel and Engel [9], using the presently best determination of the reactor spectrum and fixing $\sin^2\theta_W$ to the presently accepted value find that the measured rates in

the two energy bins given above are 1.35±0.4 and 2.0±0.5 times larger than the expected ones. Taken literally this discrepancy indicates new physics beyond the standard model. One can reconcile the data with eq. 3 by introducing a neutrino magnetic moment $\mu_\nu = (2-4)\cdot 10^{-10}$, of the right order for the spin flip mechanism in the sun to occur! Of course, the experiment is very difficult, and the discrepancy may be due to an instrumental problem.

More recently, a group from the Kurtchatov Institute in Moscow has also successfully observed $\overline{\nu}_e e^-$ scattering [37]. The detector consists of seven identical cells, and filled with a C_6F_6 based liquid scintillator (103 kg in total), with low hydrogen content, which serves as active target material. These cells are viewed by two photomultipliers, one on each side, connected by long light guides to suppress the background from the glass. All the materials chosen are radiochemically very clean, to reduce the background from natural ^{40}K, ^{232}Th and ^{238}U activities, and are essentially hydrogen free, so that there is little background from the reaction $\overline{\nu}_e + p \rightarrow e^+ + n$. The detector is surrounded by various shielding layers to reduce the background from local activities. A plastic scintillator, placed on top of the shieldings, suppresses the background from the cosmics. The neutrino flux, at the detector site, is $3.4\cdot 10^{12}\ cm^{-2}s^{-1}$.

So far, data have been taken for 250 days with reactor on, and 80 days with reactor off. The difference gives the reactor associated signal, which is clearly present above 3.15 MeV electron recoil energy, as can be seen from table 2. It is estimated that 0.1 $event/day$

Table 2: Event rate in the Kurtchatov experiment

$T(MeV)$	Events/day		
	Reactor on	Reactor off	on-off
3.15-5.17	8.27 ± 0.18	7.49 ± 0.31	0.78 ± 0.36

comes from the background of the reaction $\overline{\nu}_e + p \rightarrow e^+ + n$, the remaining 0.68±0.36 being due to $\overline{\nu}_e e^-$ scattering. This rate is compatible with expectations, obtained with $\sin\theta_W = 0.23$, and leads to the limit $\mu_\nu < 2.4\cdot 10^{-10}$ for the neutrino magnetic moment. This results is not in conflict with the UC Irvine one.

It clearly appears important to improve by a large factor on these results, and clarify the situation. We propose to measure $\overline{\nu}_e e^- \rightarrow \overline{\nu}_e e^-$ scattering with much better precision.

We are planning to use a gas time projection chamber (TPC), the drift volume of which serving as electron target. We should thus be able to identify well single electrons originating from inside a predefined fiducial volume. Such a good signature should help in keeping the background down. For instance, multi-Compton events inside the drift volume can be rejected. Beta activities from the walls will be identified as such.

Since we have tracking, we can measure the scattering angle φ_e of the electron. It is not so small at these energies:

$$cos\varphi_e = \frac{T(E_\nu + m_e)}{p_e E_\nu} \text{ (p_e is the electron momentum),}$$

and multiple scattering is non negligible. So this will only give a modest background suppression. But it will allow a simultaneous measurement of signal plus background events in the forward direction and background events only in the backward direction. Background can thus be measured on-line, while the reactor is on. This is particularly important in the case of a non optimal signal to background ratio, since the reactor off periods are in general too short to reach good statistical precision.

We note that part of the SRP background was due to natural activities. Much progress has been accomplished these recent years in low background techniques, and cleaner materials are available. The materials to be used must, in addition, also have little cosmogenic activation, since all power reactors are aboveground.

We will use a hydrogen free medium for the detector, so we will completely suppress the background from $\overline{\nu}_e + p \rightarrow e^+ + n$ scattering.

One of the essential features of the SRP detector was the good anti-Compton rejection which must be retained in a new design. For this, our TPC will be immersed in a liquid scintillation detector.

The detector must be placed near a reactor as powerful as possible to maximize the $\overline{\nu}_e$ flux, and as close as possible, keeping the reactor correlated background at an acceptable level. The reactor correlated background must be negligible. The Bugey reactor (2800 $MWth$) appears ideal. It has for a long time been used to search for neutrino oscillations [38] - [41]. It emits about $5 \cdot 10^{20}$ $\overline{\nu}_e$ s^{-1} and is on 11 months out of 12. A lab has been installed underneath the core, with a room large enough for the detector at a distance of 18.6 m from the core. This is the preferred location for the experiment. The access is not very easy however for larger components, which will impose some constraints on the design of the experiment.

II. GENERAL DETECTOR CONCEPT.

The general concept of the experiment has been described previously in a letter of intent [42]. The tracking detector is a 1 m^3 time projection chamber (TPC) and is conceptually similar to the Xe TPC presently operated in the Gotthard underground lab by the Caltech-Neuchâtel-PSI collaboration [43].

The gas should have low Z to minimize multiple scattering, and have a high electron density. Among noble gases Ne seems to be the best compromise. But even more attractive appears CF_4, which has a very high density (3.68 $g \cdot l^{-1}$ at 1 bar and thus a very high electron density ($1.06 \cdot 10^{21}$ cm^{-3} at 1 bar), larger than that of Ne for instance. We will work at 5 bar of pressure, and have a total number of target electrons of $N_e = 5.29 \cdot 10^{27}$. The radiation length $X_0 = 35.9$ $g \cdot cm^{-2}$ is acceptable. Its drifting properties have been studied by various authors (see ref. [44] for a summary), and in particular by Schmidt and collaborators in Heidelberg [45]. The drift velocity is very high, $\sim$4 $cm \cdot \mu s^{-1}$ for an electric field of 600 $V \cdot cm^{-1}$ at 5 bar. The total drift time for a distance of 1.5 m would thus be 38 μs, making the detector reasonably fast. The lateral drift is small and would amount to 2.5 mm after 1 m at the same field strength. The longitudinal drift, 2.2 mm would be somewhat less.

All these parameters have been obtained from measurements at 1 bar and over a drift distance of a few cm. We have shown however that electrons can be drifted over long distances in 5 bar of pure CF_4 with a mini-TPC prototype. The drift length was 20 cm and the active diameter 10 cm. to achieve good purity, the gas was circulated continuously through an Oxysorb filter to remove oxygen and a cold trap to remove water and possible freon contaminations. A mean drift distance of 9^{+9}_{-3} m at 5 bar and at 600 $V \cdot cm^{-1}$ was achieved, which is good enough for our application [46]. Measurements of the drift velocity from the pulse length of through-going cosmic muons were also performed and gave 3.4 $cm \cdot \mu s^{-1}$ for an electric field of 100 $V \cdot cm^{-1} \cdot bar^{-1}$, 5.9 $cm \cdot \mu s^{-1}$ for 200 $V \cdot cm^{-1} \cdot bar^{-1}$, and 7.5 $cm \cdot \mu s^{-1}$ for 600 $V \cdot cm^{-1} \cdot bar^{-1}$, in good agreement with the values from the litterature [44]. Upper limits for the lateral drift close to the above mentioned values were also obtained.

The cosmogenic activation of C and F is reasonably low since these nuclei are light. We will elaborate more on this later. Also CF_4 is not toxic, not flammable, and relatively cheap ($\sim$2 SF per liter).

The general layout of the detector as we envision it now is shown in fig. 2. The CF_4 gas at 5 bar is contained in a cylindrical acrylic vessel of inner diameter 90 cm and 158 cm long. The drift volume is delimited by a cathode on one end of the vessel, and a grid on the other one. These, along with field shaping rings at successive potentials on the outside of the vessel cylinder, provide an homogeneous drift field. With this design, the CF_4 volume is active over its entire diameter.

Behind the grid is an anode plane. The anode wires are separated by potential wires. The inner diameter of the frame is 90 cm. All anode wires are connected together to give the energy signal. The following plane contains two sets of isolated perpendicular strips to pick up the induced signals. The pitch, 3.3 mm, is well adapted to the lateral drift

in CF_4. This $x-y$ plane provides the spatial information along the x and y axis in the anode plane. The $x-y$ plane is kept at ground potential, while the anode plane is at a positive high voltage large enough to have good amplification around the anode wires. This way the number of high voltage feed-throughs is minimal, which is important for the low background environment. The third coordinate, along the drift field (z) is determined from the time evolution of the signals. This only allows a determination relative to the point of the track closest to the grid. An absolute determination of z may be possible if we can exploit the cathode or grid signal. We are exploring this point.

To fully exploit the information provided by the TPC, it is foreseen to use a read-out electronic with fast flash ADC's for the anode and each x or y strip.

Electron tracks have been simulated and some examples are shown in fig. 3. Using the first 2 cm of the track and a non optimized procedure we have reconstructed the measured distribution of the electron scattering angle φ_e. The results are shown in fig. 4. One sees that for $0.5 < T < 1\ MeV$ φ_e is always less than 1.5 rad. At higher energies the distribution gets narrower. These distributions get only marginally wider when the finite strip spacing of 3.3 mm is taken into account.

The acrylic vessel will be immersed in a stainless steel tank filled with a mineral oil based liquid scintillator. The steel vessel will be pressurized so as to have a small pressure difference between the inside and the outside of the lucite vessel. Top and bottom lid of the vessel will be instrumented with photomultipliers. The scintillator will serve to veto the cosmic muons and as anti-Compton detector. For good anti-Compton efficiency, say of order 99 % a thickness of around 50 to 60 cm is necessary assuming a density around 0.9 $g \cdot cm^{-3}$, as well as a threshold around 100 keV. This requires a good photomultiplier coverage, about 20 % for a light transmission length of several meters, and triggering at the 10 photoelectron level, which seems doable. This corresponds to a total of some 40 photomultipliers of 20 cm diameter.

The liquid scintillator and the steel vessel will also serve as passive shielding, but will not be sufficient. It will be necessary to add 15 cm of low activity Pb around the steel vessel to reduce the local activities. Concerning the cosmic rays, the Bugey lab is in a favorable situation. It is below the core, and has a large overburden of steel, concrete and water corresponding to about 20 m water equivalent. This attenuates the muons by a factor 4, and eliminates the nucleons. Nevertheless, materials with low cosmogenic activation must be selected for the construction of the detector.

In the following chapters, a detailed description of the apparatus is made. In section III, the reactor is described. In section IV, the various detector components are presented. Signal and background rates are discussed in section V.

III. THE REACTOR AS NEUTRINO SOURCE.

A nuclear reactor is an intense and very pure source of $\overline{\nu}_e$. In average, six $\overline{\nu}_e$, are emitted per fission from β^- of neutron enriched fission fragments with a total kinetic enrgy of 11 MeV. A power reactor of 2800 $MWth$ such as Bugey 5 produces a flux of $5 \cdot 10^{20}$ $\overline{\nu}_e$ per second into 4π.

III.1 The experimental site.

The Bugey nuclear power plant is located about 40 km East of Lyon and 150 km from Geneva and has been used for a long time to search for neutrino oscillations [38] - [41]. The reactor is built on a concrete raft with large caves (fig. 5.) Experimental area (R060 and R070) have been installed in the basement of the reactor Bugey 5. The closer area R060 located at 15 m from the core where has been taking place untill end of 1992 a neutrino oscillation experiment is however not the most appropriate : we would need a new derogation to the U4 procedure which requests this area to be sanded; moreover, there is some residual reactor associated gamma and may be also neutron flux. We propose to install the detector in the area R070 (fig. 6.). This area has been the repair laboratory for the previous experiment and is equiped with electricity, and fire detection system. It is located at a distance of 18.6 m from the core, where the neutrino flux available is 10^{13} $cm^{-2} \cdot s^{-1}$. EDF has already yielded an agreement to the collaboration for the setting-up of our experiment in this area. However minor modifications to the existing installation as well as an upgrading of fire protection system have to be realized.

The gamma activity of this area measured without shielding with a same NaI crystal is slightly lower than that of the ISN laboratory. The counting rate is $0.39 Hz cm^{-2}$ for a threshold of 100 keV. This value is compatible to the counting rate of 6000 Hz for $3m^2$, measured in the neutrino oscillation experiment with a 600 l detector outside its shielding for a threshold of 200 keV. About 8 % of the gammas have an energy between 1.4 and 3 MeV, and 0.2 % at an energy higher than 3 MeV. The anti-Compton detector will expose a total surface of 25 m^2, this would lead to a total counting rate of $\sim 10^5 Hz$ without shielding. A 15 cm thick layer of Lead has a suppression factor of 3 order of magnitude and will be more then sufficient to shield against this source of background.

Nuclear reactors produce an important quantity of active gas by fission (Krypton, Xenon) and by activation of rare gas (Argon). Radioactive dusts (Cobalt) are also produced from abrasion of activated metals. Completely harmless when outside of the shielding or the anti-Compton, these contaminants and in particular single beta emitters are very dangerous when they arrive at the level of the TPC. The anti-Compton is air tight during normal running time. The experimental area is already furnished with fresh air from outside of the reactor building through filters. Special cares however have to be taken during the time of the installation of the detector and when interventions on the inner part of the TPC are necessary. After such interventions, and if it is needed, it could be possible to eliminate any residual radioactive gas by filling the chamber with a purified gas

and then empty it down to a good vacuum. A NaI monitor will be operated permanently to measure the ambiant radioactivity and to signal any abnormal increase of activity in the air.

Reactor associated gamma flux have been measured with an NaI crystal (4" high and 5" in diameter) outside shielding in the area R060 at 15 m from the core of the reactor. The counting rate difference between reactor on and off is $0.026 \pm 0.002 Hz$ for neutron capture gamma rays ($E_\gamma > 3.5 MeV$). In R070, at 18.6 m from the core, where we shall install the experiment, there will be twice more ($6m$ instead of 3 m) concrete shieldings against radiations from the core, the residual gamma flux will be completely insignificant. No neutron flux associated with the reactor has been measured in the BUGEY-I experiment. An upper limit of 20 $n \cdot h^{-1} \cdot m^{-2}$ could be deduced from the uncertainties of measurements. Such flux of neutrons, if it really exists would be completely suppressed by the supplementary 3 m of concrete. The basement of Bugey has an overhead loading of material equivalent to about 20 m of water. The cosmic muon flux is suppressed by a factor 4. The muon counting rate is 31.6 $s^{-1} \cdot m^{-2}$.

III.2 The reactor spectrum

Reactors have been used extensively over the recent years as neutrino sources for various experiments. Much attention has been devoted to the reactor spectrum. The neutrinos are produced in the β decay of the fission fragments. In a pressurized water reactor (PWR) such as Bugey the fragments of ^{235}U, ^{239}Pu, ^{238}U and ^{241}Pu contribute 55 %, 33 %, 7 % and 5 % respectively on average. The time dependence in the reactor cycle is weak and well known [33]. The BUGEY-II experiment [40] was dedicated partly to the study of this effect. Neutrino flux were measured at seven periods along an annual burning cycle. The changes of neutrino event rate were in good agreement with predictions deduced from the burn-up evolution provided by EDF.

The $\overline{\nu}_e$ spectrum for each one of these isotopes must be determined. Two approaches have been taken. One is to calculate the spectrum from the yields and decay schemes of the fission fragments. At low energy long lived low endpoint fragments with well known yields and decay schemes dominate so that the calculations are relatively straightforward. At higher energy however short lived nuclei with poorly known or totally unknown yields and decay schemes become more important. Models have to be used which limits the accuracy. The more recent and more elaborate of these calculations achieve a precision of a few percent below 2 MeV and around 20% at 8 MeV [47], [48], [9]. The general feature is a rather smooth distribution peaking around 0.5–1 MeV and extending up to 8–10 MeV.

The other more pragmatic approach consists in measuring the β spectrum of the fission fragments of a given isotope, and to use that information to derive the corresponding $\overline{\nu}_e$ spectrum. The best measurements to date have been performed at the Institut Laue-Langevin in Grenoble. Thin targets of fissile isotopes sandwiched between Ni foils to contain the fission fragments were exposed to a high flux of thermal neutrons near the core

of the reactor. The energy of the β's was measured using the BILL magnetic spectrometer. The major isotopes ^{235}U and ^{239}Pu, as well as ^{241}Pu have been investigated this way [49], [50], [51]. The precision on the β spectra is around 2 % for kinetic energies above 2 MeV. Essentially these spectra are superpositions of a large number of β decays with allowed shape P_β. They can however be approximated well by a superposition of a limited number of them, say 30:

$$N_\beta(E_e) = \sum a_i P_\beta(E_e, E_0^i, Z^i). \tag{6}$$

The endpoint energies E_0^i are chosen at regular intervals. The distribution of Z^i, the charge of the fission fragment, as a function of the endpoint energy is taken from experimental data. The yields a_i are varied until good agreement is found with the measured spectrum. The $\overline{\nu}_e$ spectrum is then obtained from the same set of a_i:

$$N_\nu(E_\nu) = \sum a_i P_\beta(E_0^i - E_\nu, E_0^i, Z^i). \tag{7}$$

This procedure was shown to introduce very little additional uncertainty. The spectra determined this way have uncertainties around 3 % between 2 and 8 MeV, much better in the upper part of that window than those of calculated spectra, with which they agree within errors.

For ^{238}U which has a large fission cross-section for fast neutrons no such measurements exist and one has to rely on calculations. Fortunately ^{238}U does not contribute much ($\sim$ 7% in a PWR) to the total spectrum and adds only little to the error. That total reactor spectrum is the weighted average of all the spectra of the individual fissile isotopes. Its uncertainty between 2 and 8 MeV is thus also around 3% (68 % confidence). For energies below 2 MeV the calculated spectra must be taken which, in that energy range, also have uncertainties of order 3%.

It should be added that these spectra allow to reproduce well, within an uncertainty of 6 %, the e^+ spectra from the reaction $\overline{\nu}_e p \rightarrow e^+ n$ observed in the Goesgen and BUGEY-I experiments [33], [52], assuming no neutrino oscillations.

The energies released per fission have been measured with good precision [53], but there is a further source of uncertainty on the normalization of the $\overline{\nu}_e$ reactor spectrum: the power of the reactor in general is known to within 2 % only. In all, thus the error on the reactor spectrum in the energy range is of order 3.5 %.

For energy lower than 1.5 MeV we should take into account $\overline{\nu_e}$ coming from β^- decay of ^{239}U ($Q_\beta = 1.266 MeV$) and ^{239}Np ($Q_\beta = 0.721 MeV$). The associated intensity of $\overline{\nu_e}$ is directly related to the production of ^{239}Pu and can be accurately evaluated. In the previous discussions, we have neglected the neutrino flux due to activation of materials of the internal structure of the core. In a PWR type power reactor about 2 % of neutrons are captured by materials of the internal structure (Zircalloy and stainless steel) and 2 % of neutrons are leaking outside the core and will be captured by reactor tank also made out of stainless steel. Most of the neutron activation products will lead to stable nuclei after dexcitation by gamma emissions. Only a small fraction will yield $\beta^\pm$ emitters or electron captures. The associated neutrino flux can be estimated from the composition of the materials. The ratio of $\overline{\nu}_e$ from activation to $\overline{\nu_e}$ from fission with energy higher

than 500 keV has been evaluated to be a fraction of 10^{-3} and the ratio of ν_e / $\overline{\nu_e}$ to be a fraction of 10^{-4}. These values are consistent with results obtained for the ILL reactor [54].

IV. DETAILED DESCRIPTION OF THE DETECTOR.

IV.1 Acrylic vessel.

The TPC vessel, a cylinder with inner length 158 *cm* and inner diameter 90 *cm*, is made from acrylic, a material which can be procured with very low level of activity. The walls have to be thick enough to withstand the pressure difference between the scintillator and the gas, which will be kept as low as possible, but no more, in order not to absorb too many photons, which would reduce the efficiency of the anti-Compton. A thickness of 1 *cm* for the cylinder itself and of 2 *cm* for the lids seems a good compromise.

We verified that the outgassing of acrylic does not lead to a degradation of gas purity leading to reduced attenuation length or energy resolution. For this, a prototype TPC with acrylic containement vessel has been constructed in Gran Sasso. The TPC, including its gas purification system, is otherwise very similar to the mini-TPC with steel containement operated in Neuchâtel for other tests, and described in [55]. The TPC has been successfully operated with CF_4 up to a pressure of 5 *bar*. The attenuation length was measured with a ^{55}Fe source moved inside the chamber. It was found to be 9^{+9}_{-3} *m* at 5 *bar*, as large as in the mini-TPC with steel containement.

In addition, the cage of *Cu* field shaping rings in the Neuchâtel mini-TPC has been replaced with an acrylic cylinder of diameter 15 *cm*. The field shaping rings are painted on the outside with silver paint, and are connected with resistors. Good muon tracks, such as those shown in section IV.3, have been obtained with 5 *bar* of CF_4. This is a second, less quantative, proof that the gas quality can be maintained in a an acrylic vessel. It also shows that it will be possible in the final TPC, to mount the field shaping rings on the outside of the acrylic vessel, which will thus be active over its entire diameter.

IV.2 Gas purification.

The gas will be purified in the same way as in the prototype TPC's. Before filling, the system is evacuated to high vacuum (at least 10^{-5} *mbar*) with a turbo pump. The gas introduced into the chamber is the cleanest CF_4 commercially available (99.999% pure). To achieve and maintain the required purity, the gas will be circulated in closed circuit through an Oxisorb filter to remove oxigen and through a cold trap to remove water and possible freon contaminations. The cold trap consists of a steel spiral, immersed in an ethanol bath kept at a constant temperature of $-95°C$, just above the CF_4 boiling point at 5 *bar*.

If necessary, the gas can be recovered in a battery of cylinders immersed in liquid nitrogen, as is done presently with the prototype TPC's.

IV.3 Wire planes, $x - y$ pad.

The wire planes consist of a grid, which defines the electric drift field, along with the cathode and the field shaping rings, an anode plane, where the electrons are collected and amplified, and an $x - y$ plane, which picks up the induced signal, used for the spatial information along the x and y axis. The information along the z axis parallel to the drift field is derived from the time evolution of the signals.

The grid and the anode plane are mounted on the same frame, and are separated by a 9 mm gap. The distance between grid wires (100 μm W wires) is 4.66 mm. The anode wires (20 μm W wires) are separated by potential wires (100 μm W wires). The distance between anode wires, and potential wires, is also 4.66 mm. All wires are mounted with crimps, a method successfully used in the NEMO detector [56]. We prefer this solution to soldering the wires on background reasons. All solders, to our knowledge, contain to a certain degree ^{210}Pb, which gives rise to bremsstrahlung γ rays from β activity below 0.5 to 1 MeV. The wires are positioned with pins, which should give a precision better than 20 μm. We are presently building a small scale prototype of the anode plane, using the crimping technique, to be tested in the mini-TPC. It is shown in fig. 7. The final plane will be very similar, except of course for the overall diameter, and will have an additional Cu or carbon fiber reinforcing ring.

The x-y plane consists of a 100 μm thick PET foil stretched on a frame, to be fixed to the anode frame. The x strips are deposited on one side, the y strips, of course crossed, on the other one. To reduce the capacitance, the same pattern as in the prototype, shown in fig. 8, will be used. The strips are placed so that the overlap is minimal. The pitch, distance from strip to strip, is 3.3 mm. The distance from the anode to the x-y plane is 3 mm. This construction avoids heavy mounting pieces, which would absorb γ's, and reduce the anti-Compton efficiency.

From the electrical point of view, the planned planes are close to those in the Gotthard ^{136}Xe TPC, which give good anode and $x - y$ signals. Also, a prototype $x - y$ and anode plane, made with classical mounting techniques, but very similar otherwise, has been built for our mini-TPC. The x and y pitch is 2.8 mm, and the anode one 4.0 mm. It has been successfully tested at 5 bar of CF_4, with a drift field of 500 $V \cdot cm^{-1}$. Examples of cosmic muon tracks obtained with the simple discriminator scheme used in the Gotthard ^{136}Xe TPC are shown in fig. 3. The spatial resolution along the x and y axis is around 3 mm (1 σ). Along the z axis, it is of order 7 mm. The limitation in this case comes however from the high drift velocity in CF_4 ($\sim 3.5 - 4$ $cm \cdot \mu s^{-1}$), combined with the relatively slow response of our electronics. This can be much improved by using a more sophisticated read-out electronics, such as that we are planning to use, with flash ADC's running at 25 MHz.

IV.4 Read-out electronics.

Flash ADC's (FADC) will be used to read-out the pick up plane and the anode plane. The FADC channels will be coupled to the $x-y$ strips via preamplifiers based on LeCroy TRA1000 hybrid circuits. A drifttime resolution, giving a position resolution along the TPC axis of about 1 mm, will be achieved by sampling the preamplified signals. A position resolution of about 1 mm in the transverse plane will be achieved by calculating the center of gravity of the signal amplitudes on neighbouring strips as a function of drifttime.

For an electron drift velocity of 4 cm/μs in 5 bar CF_4 gas the FADC system has to be operated at a 25 MHz sampling frequency, corresponding to 40 ns sampling time. In order to cover the maximum drift length (1.58 m) a memory depth of 1024 words is required. We plan to use the commercially available Struck DL350 FADC system, which fullfills these criteria. To read out the entire $x-y$ plane 514 channels are necessary. The ADC's will be running continuously, and will be read out when a signal above threshold is detected on the anode. Measurements are currently being performed with a FADC test system and the mini-TPC; 25 x and 25 y channels are instrumented.

In the following, we give some more detailed information on the configuration we envision. Figure 11 shows the DL350 Struck Flash ADC system with VME read-out. The CPU will be replaced by a Macintosh IIfx for control and monitoring. The Mac is linked to the VME crate via a MacVee VME controller (located in the VME crate) and the Micron card (located in the computer). Up to 24 FADC DL363 modules (192 channels) can be operated in a single DL350 FADC crate. Three of the four additional slots are occupied by the sampler (DL352), the tester (DL303) and the scanner and hit detector (DL357) which is a VME interface performing zero suppression. The DL363 module digitizes 8 channels in parallel with a maximum possible sampling rate of 100 MHz and a resolution of 8-bit. A non-linear response function can be used to increase the amplitude resolution on small signals. The DL363 has a memory of 1024 words per channel. For 600 channels, 3 DL350 crates and one VME crate are necessary.

The sampler module DL352 is the central timing controller in a DL350-System. It consists of a programmable clock (6.25, 12.5, 25, 50 and 100 MHz), address counters and a set of registers for start/stop control. The system will be operated in a Common Stop sampling mode. After reception of a START command the sampler generates Data Strobes (DS) and increments its address until it is stopped by an external front panel STOP pulse (trigger signal from the anode wires of the TPC).

A DL350 FADC/VME system is currently being operated by the Obelix collaboration at CERN/LEAR. We have tested such a system by CAMAC using an external pulse generator or the DL303 tester as an analog signal generator. A program using the Think-C Mac package was used for control and monitoring and for online analysis and display of the data. Results obtained with a 25 MHz sampling frequency will be discussed.

To achieve a good time resolution the rise time of the pulse should be long compared to the 40 ns sampling time (at least 100 ns), to determine accurately the drifttime. The FADC's cover an input voltage range from 0 to 600 mV. Two test signal were used, one

directly from the external pulser (rise time 100 ns) the other from one of the preamplifiers (rise time 300 ns). Both amplitudes were normalized to 130 mV. Figure 12 shows both analog signals. The corresponding digitized signals are plotted in fig. 13 as a function of time. Only the first 128 bins among 1024 are shown, one bin corresponding to 40 ns. About 8 time samplings can be obtained from the preamplifier (fig. 13b). This corresponds to ~300 ns rise time and allows a good determination of the time and amplitude by pulse shape analysis. The procedure was repeated with different input amplitudes.

We are confident that the proposed configuration, with this read-out electronics, will give sufficient spatial information. In particular, it will allow to determine the original direction of a track from its 2 first centimeters, before the spread from multiple scattering is too large. Thanks to the low activity shieldings and on-line veto against cosmics, the trigger rates is expected to be low (a few Hz), the data taking will not be a major problem. To further reduce the size of the data to be stored, on-line zero-suppression will be applied.

IV.5 Anti-Compton, scintillator, light collection

The anti-Compton will be essentially a quasi hermetic coverture of liquid scintillator (NE235H or equivalent) around the TPC chamber. The thickness is 60cm for the ends, and 50cm on the cylindrical periphery. The liquid scintillator NE235H is a familiar product of Nuclear Enterprise. It is based on mineral oil and is compatible with acrylic. It can be procured with a transmission length of more than 10 m, and a light yield of 50% anthracene. The 38 photomultipliers (8" EMI 9351 low activity tubes) will be attached on two frames to form two concentric circles at each of the ends. Surfaces between photocathodes will be painted with titanium oxyde (TiO_2)or covered with a thin teflon sheet for light reflection. The phototubes will be directly immersed into the liquid for optimum light coupling.

A good light collection is crucial for the experiment. To reach the anti-Compton rejection efficiency required, the detector must be able to trigger at a threshold of 100 keV. The light collection has been studied by Monte-Carlo simulation [57] taking into account the geometries of the vessel, TPC and photocathodes, the light emission spectrum and attenuation lengths of the liquid scintillator as well as the quantum efficiency of the phototubes. With cylindrical walls acting as specular reflectors and end faces as diffuse reflectors (TiO2), the total number of photoelectrons collected for the most unfavorable points at the medium plane of the anti-Compton would be 140 per MeV, distributed over the 38 phototubes. This number could be increased by 65% to 234 photoelectrons per MeV by using total reflection. The reflectors considered for this are double curved lucite panels, sealed on the edges, separated by an air gap and a highly reflecting aluminum foil. The configuration preferred for the simplicity of its realisation is the one with cylindrical walls painted also with titanium oxyde, the number of photoelectrons expected is in this case 184 per MeV. An alternate version in which the photocathodes are surrounded by large parabolic specular reflectors, covering 3 times the surface of the photocathode, does

not lead to a significant improvement. This is because the additionnal light collectors disturb the existing diffuse reflectors. An anti-Compton prototype (1 m long and and 0.46 m in diameter equiped with a 8" phototube) has been built in Grenoble to study more in details the light collection.

This prototype is also used to measure experimental rejection efficiencies at different energy thresholds. A NaI cristal can be intoduced into the center of the Anti-Compton prototype. It then simulates the TPC and detects gamma rays from an external calibrated source with and without the rejection of the anti-Compton.

In the experiment, the anti-Compton will trigger at three levels on the sum signal of all phototubes. The first threshold, at around 100 keV, will give the anti-Compton signal. A second signal will be produced above 1 MeV. This signal will come with most positrons produced in the reaction $\overline{\nu}_e + p \rightarrow e^+ + n$. And there will be a third threshold at several MeV, signaling cosmic muons. For complete information, each PMT will in addition be fed into a FADC channel similar to those for the $x - y$ plane.

IV.6 Steel vessel, shielding.

The container of the liquid scintillator will be a stainless steel vessel of cylindrical shape (2.80 m long, 2 m in diameter), designed to support a pressure of 5 bar. The wall of the vessel will be about 1 cm thick and will be reinforced at regular distances so as to be able to support the lead shielding of 15 cm thickness. To reduce the neutron flux created in the lead by the cosmic muons, there will be a layer of 10 cm of borated polyethylene surrounding the steel vessel. The vessel and the shielding will consist of a fixed central part and two movable doors to allow access to the TPC and the phototubes. A drawing of the detector and the shielding is shown in fig. 10. A commercial company will be involved in the design and construction of the vessel. For safety reasons, the vessel will be equiped with two calibrated valves to prevent any accidental overpressure. The safety valves as well as the normal purging valve will lead to a ballast container of 8 m^3 which will be installed in the room next to the experimental area. This ballast will also be used as storage when draining the vessel.

A pressurization system will be installed which maintains a differential pressure as small as possible between the acrylic vessel and the liquid scintillator. The 5 bar of pressure in the CF_4 will essentially be supported by the steel vessel. This system will be tested on a medium scale prototype, built in Padova, comprising a stainless steel vessel of 80 cm diameter, and 90 cm height, with an inner acrylic vessel of 40 cm diameter, and 50 cm height. The steel vessel has acrylic windows, so that PMT's can be mounted.

IV.7 Material activities.

To maintain the background at an acceptable level, all components must be made from radiochemically clean components. The contamination level must be particularly low in materials entering in large quantities, like the liquid scintillator. The choice of materials for the different components is discussed in the following.

The materials close to the detector entering in large amounts are the acrylic, and the liquid scintillator. We will choose a mineral oil based scintillator, such as NE235. Mineral oil can be procured with a concentration in Th and U well below 10^{-12} g/g [58]. This level can be maintained in the scintillator, since the additives (pseudo-cumene) are also very clean [59]. In any event, we will test samples of the scintillator to be used on a mass spectrograph in Mainz, sensitive to concentrations as low as 10^{-12} g/g.

The radioactivity of acrylic has been measured in the germanium detector placed in the underground low activity facility of the Gran Sasso Laboratory [60]. The activity of the acrylic has been found to be below the sensitivity of the germanium detector ($\sim 10^{-9} g/g$ for U and Th). Different techniques have been developed by the SNO Collaboration [61] to determine ultra low concentrations of Uranium and Thorium. It was shown that acrylic sheets with a concentration in U and Th of $\sim 10^{-12}$ g/g are commercially available. This more than fullfills our needs.

The CF_4 gas itself enters in much smaller quantity, and can be cleaned very efficiently. Our gas purification scheme, with a cold trap, should remove all Radon contamination, in particular if we use active charcoal, or brass wool [62]. We have verified with our mini-TPC that Rn can be removed even at $-95°C$, the temperature at which we are working. It must also be mentioned that with the imaging capability of the TPC, in particular the ease with which it sees α particles, and with the anti-Compton, the decays of Radon daugthers can be identified to a large extent, approaching 90 %. Only those decays where one single β is emitted escape identification.

Small components for the TPC such as epoxy frame, resistors, screws, connectors, O-rings and so on can be tested to a purity of 10^{-8}-$10^{-}9$ g/g with low background Ge detectors. We have access to two such detectors, in Gran Sasso and Neuchâtel, which we will use to select components.

The phototubes and the steel of the external vessel are further away. Nevertheless, they must be selected with care. We have chosen low background EMI 9351 phototubes for the anti-Compton: the concentrations in Th, U and K are $2 \cdot 10^{-8}$, $2 \cdot 10^{-8}$, and $3 \cdot 10^{-5}$ respectively [59].

The most dangerous radioactive contaminant of stainless steel is ^{60}Co, because of the 1.17 and 1.33 MeV γ rays emitted in its decay. In the measured sample produced by CSM-Rome a contamination of $9.6 \cdot 10^{-19}$ g/g has been found, which corresponds to an activity of 0.04 Bq/kg. The best measured sample has a contamination in Cobalt 6 times lower, it is from Kunze (Germany). It is carbon steel however, and we have to verify that this is suited for our purpose. For all the measured lead samples upper limits for activity due to the components of the U and Th chains in secular equilibrium are of the order of

10^{-11} g/g. This is rather low, and should not be at the origin of any significant background in our experiment. However, there is a very different contamination of ^{210}Pb, which, with its daughter nuclides ^{210}Bi and ^{210}Po, is responsible for the intrinsic radioactivity of lead. In particular, the energetic (1.16 MeV) beta rays of ^{210}Bi induce characteristic X-rays and bremsstrahlung in the energy region below 1 MeV.

The activity due to ^{210}Pb is of about 190 Bq/Kg in modern lead and below 1 Bq/kg in old Roman lead and special low radioactivity lead [63].

V. SIGNAL AND BACKGROUND.

V.1 Event rate, simulation

The expected rates at 18.6 m from the 2800 $MWth$ Bugey reactor have been calculated using eq. 3, assuming W and Z exchange only, and are given in table 3. The acceptance for fully contained electrons was estimated by Monte-Carlo simulation using the GEANT code. These rates have to be compared to background rates, which are estimated in the following.

Table 3: event rates assuming weak interaction only

$T(MeV)$	Acceptance (Contained)	Events/day $\overline{\nu}_e e^-$
0.5–1	0.85	5.1
> 1	0.65	4.6

The background events originating from the various sources described in the following paragraphes were simulated by Monte-Carlo method using the code GEANT [65]. The simulation was focussed on β and γ rays issued from different parts of the detector, since they are by far the dominant generators of a single electron recoil in the TPC. Such an event was defined by an energy deposition threshold of 500 keV in the gas, together with a maximum energy deposition of 100 keV in the anti-Compton liquid scintillator. Further requirement was the fully containment of the electron track with a direction of emission opposite to the reactor. Due to the possible lack of precision in the case of the lowest inefficiencies, the results were cross-checked in different ways. Firstly by comparing them to the results obtained with another Monte-carlo code [66], secondly by smoothly extrapolating the results obtained by slowly varying several parameters of the detector (size, thickness of liquid, density of media...).

V.2 Background from cosmic muons

While cosmic rays crossing the detector will be easily identified and rejected, muon interactions in the surrounding material or in the detector itself can create long-lived radioactive nuclei in the TPC, generating electron-like background events. Interactions within the fiducial volume can produce activity in two ways: stopped muons leading to capture, and inelastic scattering of through-going muons inducing production of spallation nuclei. These interactions of muons within the large amount of surrounding material (shielding, scintillator) produce neutrons (and gamma rays) which can penetrate the TPC and be absorbed.

V.2.1 Cosmic rays flux.

The experimental site in Bugey is located below concrete shielding, and protected from cosmic rays by about 2000 $g \cdot cm^{-2}$. At this depth the soft component (hadronic and electromagnetic), which amount for 1/4 of the total flux at see level, is negligible. It is almost completely attenuated in the first 1000 $g \cdot cm^{-2}$ [67]. The muon flux, with mean attenuation length around 1400 $g \cdot cm^{-2}$ at this depth, was measured at the Bugey site by the present running experiment and is 32 $\mu \cdot s^{-1} \cdot m^{-2}$. The whole detector has a projected area of 15 m^2, one then expects an overall counting rate from muons in the anti-Compton of $480Hz$. After attenuation in lead and liquid the flux of muons impinging the TPC will be $N_\mu = 2.4 \cdot 10^6 \mu \cdot m^{-2} \cdot day^{-1}$. Nearly 0.12% of these muons will stop in the CF_4. Since 45% of them are negative, one is left with $N_\mu = 4.4 \cdot 10^3$ stopped negative muon per day in the fiducial volume.

V.2.2 Stopped muons.

In low Z materials most of stopped muons will decay ($\tau = 2.2\mu s$) and the 'prompt' electron will be rejected. The probability P of muon capture versus decay depends on an effective charge Z of the material as $P = Cte \cdot Z^4$. Typically $P = 17\%$ in ^{16}O [68]. A μ^- is captured by a proton of nucleus as $\mu^- + (Z, A) \rightarrow (Z-1, A)^* + \nu$; the excited residual nucleus then decays by particle emission, mostly neutrons [69]. In mixed compounds as CF_4 muon captures are distributed around ^{12}C (14%) and ^{19}F (86%) nuclei [70]. This leads to 37 captures per day in ^{12}C and 980 in ^{19}F. In the case of fluor the excited residual nucleus decays mostly ($\sim 75\%$) to stable isotopes of oxygen. More troublesome are the formations of $^{19}O(Q_\beta = 4.6MeV, T_{1/2} = 27s)$ with 0 neutron emission, and $^{18}N(Q_\beta = 13.9MeV, T_{1/2} = 0.63s)$ with proton emission. These two nuclei will be produced at a rate of respectively 127 and 98 per day. However these β decays are always accompanied by one γ at least. The inefficiency of the anti-Compton ($2 \cdot 10^{-2}$) will leave us with respectively 2.5 and 2 background events per day. The tracking rejection of the TPC (angle, threshold, and track containment) will allow to lower the rate of those events to respectively 0.45 and 0.2 per day. At the same time μ^--capture on Carbon leading to $^{12}B(Q_\beta = 13.4MeV, T_{1/2} = 0.02s)$ which is the more dangerous since it is a pure beta decay, can be estimated in a similar way to 3.7 ^{12}B formed per day, lowered to 0.37 per day with tracking rejection. The total rate of bakground events from muon capture in the gas is then estimated to$\approx 1 \cdot day^{-1}$. In addition the short half-life of ^{12}B and ^{18}N allows vetoing by a signal of a few *sec* starting at the detection of a stopping, non decaying μ^- in the TPC. This number can then be reduced to

$$N_1 = 0.45 \cdot day^{-1}.$$

V.2.3 Interaction of through-going muons.

The production of unstable long-lived nuclei by inelastic scattering of muons is not easy to calculate due to the many nuclear processes involved. An estimation has been drawn as the

following. Data on muon-induced neutron production exist for underground experiments [71]. The energy dependence of this neutron production is known to vary as $< E >^{0.75}$ [72]. One can reasonably expect that the neutron production reflects the nuclei production. Long-lived $A = 12$ beta activity induced by through-going muon interacting with ^{16}O was measured at Kamiokande [73]. It was observed there that 95% of muon interaction lead to prompt events, and less than 5% to delayed beta activity. The neutron production at this depth is around $3 \cdot 10^{-4} neutron/\mu \cdot g \cdot cm^{-2}$, for muons with mean energy around 200 GeV. In the Bugey site one expects ten times less neutron per muon due to energy dependence of the cross-section (the energy of muons at 20 m.w.e is 10–15 GeV). If neutron production reflects the number of reactions, then one expects 130 reactions per day leading to spallation-like nuclei in the gas. The number of delayed events is estimated to 5% of these reactions, say 6.5 per day. In the region of mass considered here, most of the possible produced nuclei are either stable or β^+ emitter then rejected at a 98% level through the annihilation γ's. In the present case, one expects that at most 10% are pure β^- emitter, and with the angle rejection criterion one is left with less than 0.3 background event per day. This number can be reduced to a negligible level when triggering threshold and track containment are required. For example, ^{10}Be which can be produced via $\mu - C$ reactions (C nuclei amounts only to 14% of the target) has $Q_{max} = 0.555 MeV$ and more than 90% of electrons are rejected by the 500 keV threshold. ^{16}N or ^{15}C have a high Q-value and in these cases the containment efficiency is 20%. To conclude here one thinks that such events due to through-going muons contributes to the background at a marginal level.

V.3 Neutron background

Neutrons can be considered as the potential main source of background in the proposed detector. Neutrons themselves can be absorbed in the gas, if they penetrate the TPC volume, but principally they generate 2.2 MeV γ's when absorbed by protons of the hydrogen-rich surrounding scintillator. The life-time of neutrons in the scintillator is $\tau_n = 180 \mu s$. Three sources of neutrons are to be considered: neutrons from interactions of cosmic muons in the detector (lead and liquid scintillator), neutrons from $\overline{\nu}_e - p$ reactions in the liquid scintillator, and reactor correlated neutron background.

V.3.1 Neutrons from interaction of muons in the detector material.

V.3.1.1 Neutrons production in the scintillator.

- Stopped muons. Nearly 7% of the incoming negative muon flux in the detector will be stopped in the liquid scintillator. Of these, 5% lead to muon capture in C; around 80% of the captures are followed by neutron emission. Then $5 \cdot 10^4$ neutrons per day are produced homogeneously in the liquid scintillator.

- Direct interactions. Inelastic interactions of muons produce $3 \cdot 10^{-5}$ neutron/$(\mu \cdot g \cdot cm^{-2})$. Then, in the $7.85 \cdot 10^6 g$ of liquid, these reactions generate $6.3 \cdot 10^4$ neutrons

per day.

- Neutron and γ rates. The total amount of neutrons created in the scintillator will be $N_n = 1.13 \cdot 10^5$ neutrons per day. The simulation with the MORSE code [74] shows that nearly 88.7% are absorbed in the liquid, leading to the production of $1.0 \cdot 10^5 \gamma$ per day. For these 2.2 MeV γ's, uniformly emitted in the liquid the rejection efficiency is $9 \cdot 10^{-6}$. The expected background event rate for this process is then $\sim 0.9 \cdot day^{-1}$. Vetoing for 200 μs will reduce this number down to

$$N_n = 0.30 \cdot day^{-1}.$$

  Only $1.6 \cdot 10^{-4}$ of the neutrons are absorbed in CF_4 ending with the formation of 18 ^{20}F per day. The rejection of such events will be discussed in section V.3.4.

V.3.1.2 Neutrons production in the lead shielding.

The lead shielding is 15 cm thick and out of the 480 $\mu \cdot s^{-1}$, 11.5% will stop in the lead.

- Stopped muons. Nearly $2 \cdot 10^6 \mu^- \cdot day^{-1}$ stop in lead. Almost all are captured, and the mean multiplicity of neutron emission following capture is ~ 2. Then one expects $4.2 \cdot 10^6$ neutrons produced per day.

- Direct interactions. Assuming the same mean neutron production rate as described above $(3 \cdot 10^{-5})$ in the $4 \cdot 10^7 g$ of lead, $3.25 \cdot 10^5 neutrons$ per day are produced.

- Neutron and γ rates. The neutron simulation [74],[75] shows that from the total rate of $4.55 \cdot 10^6 n \cdot day^{-1}$ produced in lead, only 28.2% are not escaping outside the detector. The profile of the neutron absorption shows that 86% of this flux is absorbed in the first 10 cm of borated polyethylene inserted between the lead shielding and the anti-Compton. The capture of residual neutrons on the liquid scintillator leads to $0.18 \cdot 10^6 \gamma \cdot day^{-1}$. Only $2.5 \cdot 10^{-6}$ of the γ's produced in this region can contribute to the background in the TPC; this amounts to 0.45 per day. About half of the stopped muons will occur in the lower part of the lead and will be detected by the anti-Compton. This number can then be reduced after vetoing to

$$N_n = 0.30 \cdot day^{-1}.$$

  This rate can be further reduced if needed with external veto counters. These counters could be the muons detectors of the neutrino oscillation experiment. Of the total neutron rate, only $2 \cdot 10^{-6}$% are absorbed in the CF_4 leading to the formation of 0.09 ^{20}F per day.

V.3.2 Reactor correlated background.

As discussed previously in section III.1, the upper limit of the neutron flux associated with the reactor is $\phi_n < 20\ neutron \cdot h^{-1} \cdot m^{-2}$ at the $13.5m$ position. This flux will be completely suppressed at the $18.6m$ position, since the concrete shieldings against radiations from the core is more than doubled here.

V.3.3 Neutrons from $\overline{\nu}_e - p$ in the liquid scintillator.

Neutrons are produced through the reaction $\overline{\nu}_e + p \rightarrow n + e^+$. At 18.6m from the core the neutrino flux is $\phi = 1.2 \cdot 10^{13} \overline{\nu}_e \cdot s^{-1} \cdot cm^{-2}$. With $N_H = 5.04 \cdot 10^{29}$ hydrogen target nuclei (in the liquid the ratio H/C = 1.77), and a cross-section $\sigma = 10^{-43} cm^{-2}$, the number of produced neutron is $N_n = 5.2 \cdot 10^4\ neutron \cdot day^{-1}$. Out of these, 95% are captured in the scintillator and $4 \cdot 10^{-3}$% in the gas. The former leads to the production of 0.48 bacgkround events from the 2.2 MeV γ's, the latter to the formation of 2.1 ^{20}F per day. However, most of the γ's are emitted with a delay time equal to τ_n after the prompt pulse of the e^+ from $\overline{\nu_e} - p$. Hence vetoing for $200\mu s$ will reject this background by a factor 3 and leads to

$$N_n = 0.16 \cdot day^{-1}.$$

V.3.4 Total background events from neutrons.

The background events from 2.2 MeV γ's sum up to:

$$N_2 = 0.30 + 0.30 + 0.16 = 0.76 \cdot day^{-1}.$$

Around 20.4 ^{20}F per day are formed via neutron capture. This nucleus is beta-radioactive ($Q_{\beta-} = 7.03 MeV, T_{1/2} = 11.4s$); however β are emitted in coincidence with a 1.63 MeV γ with 100% branching ratio. The rejection inefficiency is $7.5 \cdot 10^{-3}$ (including tracking rejection). Then originating from this process we are left with

$$N_3 = 0.15 \cdot day^{-1}.$$

V.3.5 Summary of backgrounds from cosmic rays and neutrons

The background event rate due to cosmic rays and neutrons is given by the sum of N_1 due to stopped muons (V.2.2) plus N_2 and N_3 which have just been discussed:

$$N_{bkgd} = 0.45 + 0.76 + 0.15 = 1.36 \cdot day^{-1}.$$

Table 4: Simulated background event rates from cosmic rays and $\overline{\nu_e} - p$ reactions

origin	medium	type	events/day	rejection	Total
Cosmics	Gas	^{19}O	0.45		0.45
		^{18}N	0.20	veto	~ 0
		^{12}B	0.37	μ-track	~ 0
	Liquid + Acrylic	(n,γ)	0.90	veto $200\mu s$	0.30
	Lead + Steel	(n,γ)	0.45	veto	0.30
	Gas	^{20}F	0.15		0.15
$\overline{\nu_e} - p$	Liquid	(n,γ)	0.48	veto	0.16
Total			5.8		1.36

V.4 Natural activities

V.4.1 Shielding materials and outer parts of the detector

The natural activities of acrylic, scintillator liquid, steel, phototube and lead samples have been discussed previously in section IV.7. A summary of simulated background events originating from natural activities of these materials and from the gas are presented in table 5. Since the external steel vessel is a potential source of bakground due to its large mass, the effect of two available steel samples are examined. In the case of PMT's, the quoted values are obtained for EMI tubes. In the case of lead, usual impurities mentionned in previous paragraph do not contribute significantly to the background while the bremsstralung from 1.16 MeV electrons from ^{210}Pb is considered.

The measured activities contribute to a background rate of

$$N_{bkgd} \sim 0.2 \cdot day^{-1}$$

with the Kunze steel and of $0.7 \cdot day^{-1}$ with the CSM-Rome steel. The upper limits are respectively $< 1.76 \cdot day^{-1}$ and $< 3.76 \cdot day^{-1}$. These values are mainly due to the measurement uncertainties of the K contamination.

V.4.2 Inner part of the TPC

The next source of background is natural ^{40}K, ^{232}Th and ^{238}U activity in the inner core of the detector. Compared to the scintillator the quantity of CF_4 is small, and the gas can be cleaned to a high level as discussed in IV.7. The worst background in the CF_4 above

Table 5: Simulated background event rates from natural activities

medium	concentration	inefficiency	Events/day	Total N/day
Gas	U :$< 10^{-14}$	0.22	< 0.05	
Acrylic	(U,Th):$< 10^{-12}$	$1.4\ 10^{-4}$	< 0.1	
Liquid	U :$< 10^{-12}$	10^{-5}	< 0.08	< 0.23
Steel(1)	Co:$9.6\ 10^{-19}$	10^{-7}	0.6	
CSM-	U :$< 3\ 10^{-9}$		< 0.58	
Roma	Th:$< 10^{-8}$		< 0.6	
	K :$< 3\ 10^{-5}$		< 1.45	$0.6 < N < 3.23$
Steel(2)	Co:$1.5\ 10^{-19}$	10^{-7}	0.1	
Kunze	U :$< 6.8\ 10^{-10}$		< 0.13	
	Th:$< 3.9\ 10^{-9}$		< 0.25	
	K :$< 1.5\ 10^{-5}$		< 0.75	$0.1 < N < 1.23$
P.M.T.	U :$2\ 10^{-8}$		0.06	
	Th:$2\ 10^{-8}$		0.02	
	K :$3\ 10^{-5}$		0.02	0.1
Lead	$^{210}Pb < 190 Bq/Kg$			
	Bremsstrahlung	$3\ 10^{-13}$	< 0.2	< 0.2
			(1)	$0.7 < N < 3.76$
			(2)	$0.2 < N < 1.76$

0.5 MeV comes from single β of ^{234}Pa ($Q_{beta} = 2.28 MeV$) in the Uranium chain. The Uranium level in air in rural Maryland has been measured in [64] to be $2.2 \cdot 10^{14} g/g$. One can expect a lower Uranium concentration in a purified gas. It has also been mentioned in section IV.7, that Radon can be removed with cold trap and the residual contaminations can be mostly identified and then rejected.

Other more complex components such as epoxy frame, resistors, solder, feed-throughs and so on can be tested to a purity of 10^{-8}-10^{-9} g/g with Ge detectors. This was done for the Xe TPC. This background in the CF_4 TPC can thus be estimated from the background measured in the Xe TPC in the Gotthard lab, correcting for the differences in gas and geometry. This background will be reduced further by the anti-Compton detector (factor ~100, taking into account the γ multiplicities), and is shown in table 6. It should be considered an upper limits. It is hoped that the CF_4 TPC can be made cleaner than the Xe TPC with the experience gained. In particular, cleaner resistors, developped in the meantime (factor ten lower in activity) will be used for the resistor chain, and crimps will be used instead of solder for the wires. A reduction factor larger than 2 is expected. This leads to a backgroud rate from the inner part of the TPC:

$$N_{bkgd} = 1.35 \cdot day^{-1}.$$

Table 6:

	Events/day	
	$0.5 < T < 1\ MeV$	$T > 1\ MeV$
Xe background	280	32
× gas thickness ratio (0.9)	250	29
× Area ratio (2.0)	500	58
× Anti-Compton (0.01)	5	0.6
× Angular cut (0.5, 0.3)	2.5	0.2

V.5 Signal vs background, capability of the experiment

V.5.1 Signal vs background

To conclude, the total rate from the three main components of background - namely cosmics, natural activities from the outer and inner parts of the TPC - sums up to:

$$N_{bkgd} \sim 1.36 + 0.2 + 1.35 = 2.91 \cdot day^{-1}.$$

or more conservatively to:

$$N_{bkgd} < 1.36 + 1.76 + 1.35 = 4.47 \cdot day^{-1}.$$

This is to be compared to the expected signal rate of $9.7 \cdot day^{-1}$ (see table 3)

V.5.2 Capability of the experiment

The total background rate which will be measured during two reactor- off periods (~ 2 months) is thus expected to be smaller than the signal rates in the bin $0.5 < T(MeV) < 1$ ($5.1 \cdot day^{-1}$). We remind that the background will be also determined with better precision from the event rate in the backward half sphere and subtracted. The isotropy of the backgroud could be verified by relaxing some of the selection conditions. Considering the signal rates at 18.6 m in table 3, a statistical error less than 3 % should be achievable in the bin $0.5 < T(MeV) < 1$ in one year of measuring time. Combined with a systematic error of 5 %, essentially from the reactor spectrum (3.5 %), reactor power and burn-up (2 %) and detection efficiency (3 %), this leads to a sensitivity of

$$\mu_\nu \sim 3 \cdot 10^{-11},$$

more than a factor 10 better than in previous experiments. This sensitivity is mainly dominated by the systematic uncertainties and changes only slowly as a function of the signal

versus background ratio. The limit value on μ_ν would be around $4 \cdot 10^{-11}$ if background is increased by a factor of 4.

The signal rates for the bin $T > 1.MeV$ ($4.6 \cdot day^{-1}$) is equivalent to the lower energy bin, while the contribution from the magnetic moment term is more than a factor of two lower. We will exploit the ratio of this two energy bins to reduce the systematic uncertainties. However, to attain lower limits, significantly longer data taking time would then be necessary. Also we will explore ways to improve the sensitivity by exploiting the angular information.

With some luck the threshold may be lowered more, say down to 300–350 keV, and a sensitivity around $2 \cdot 10^{-11}$ seems then achievable. Depending on the actual background situation it may be possible, after the first data taking period at 5 bar, to lower pressure and threshold without loosing too much in event rate since the electron recoil spectrum peaks at low energies. That would improve the μ_ν sensitivity even more.

VI. OTHER EXPERIMENTS WITH THE MUNU DETECTOR

The TPC projected for the study of $\overline{\nu}_e e^-$ scattering at the Bugey reactor is in fact, with its tracking capability, a general purpose low energy, low background detector. It could be used, with minor modifications, for other applications in particle physics. Two of these are described in the following, they concern the search of neutrinoless double beta decay, and the search for dark matter particles.

VI.1 Neutrinoless Double Beta Decay

The study of neutrinoless double-beta-decay ($0\nu\beta\beta$) provides a test of the fundamental properties of the neutrino, its mass, and its behaviour under charge conjugation [12]. This decay requires a non-vanishing Majorana mass for the neutrino, and has been searched for in various candidates nuclei. Presently the best limits for the half-lives, summarized in table 7, have been obtained with a solid-state detector using Ge enriched in ^{76}Ge by the Heidelberg-Moscow collaboration [76], and a gaseous detector, a TPC, filled with Xe enriched in ^{136}Xe by the Caltech-Neuchâtel-PSI collaboration [43]. These limits can be

Table 7: Limits (90 % CL) on neutrinoless double beta decay.

	$T^{0\nu}_{1/2}$
^{76}Ge	$> 1.4 \cdot 10^{24}\ yr$
^{136}Xe	$> 2.5 \cdot 10^{23}\ yr$

translated into limits for the effective Majorana mass of the neutrino $< m_\nu >$, using calculated nuclear matrix elements. Limits derived with the most recent calculations are given in table 8. The fluctuations between calculations can be as much as 2.5, which gives

Table 8: Limits on $< m_\nu >$.

	Caltech [77]	Heidelberg [78]	Tuebingen [79]
^{76}Ge	<3.3–4.6	<1.5	<1.7
^{136}Xe	<3.2–4.9	< 3	< 3

an idea of the associated uncertainties. In view of these, it appears important to search for double beta decay in more than one nucleus.

These experiments are continuing, they may, in a reasonable amount of time, extend their half-life sensitivity to $1 \cdot 10^{25}\ yr$ for ^{76}Ge, and say $2 \cdot 10^{24}$for ^{136}Xe. Since the half-lives scale with $< m_\nu >^2$, one will reach a sensitivity to $< m_\nu >$ of order 0.6–1.5 eV.

The $\overline{\nu}_e e^-$ TPC is an improved version of the Xe TPC. The Xe TPC has an active volume of 200 liters, and operates at 5 bars with Xe enriched to 62.5 % in ^{136}Xe. The

active volume of the $\overline{\nu}_e e^-$ TPC is 1000 liters, and can be pressurized to 5 bars as well. Filled with the same quality Xe, it would have 5 times more ^{136}Xe atoms than the Xe TPC. The efficiency for contained events at 2.48 MeV, the transition energy of $0\nu\beta\beta$ decay, would be 50 %, while that of the Xe TPC is 31 %. The effective quantity of ^{136}Xe atoms would be around $4 \cdot 10^{25}$. Thanks to the anti-Compton and, to a lesser extent, the selection of cleaner materials, the background would be around 100 times less, in other words, essentially inexistent for the search of $0\nu\beta\beta$ double beta decay. This would result in a sensitivity around

$$T_{1/2}^{0\nu} \sim 2 \cdot 10^{25} \ yr,$$

in about one year of measuring time, an improvement by an order of magnitude, in comparison with the capability of the present experiment. Correspondingly, the sensitivity to the neutrino mass would extend down to

$$< m_\nu > \sim 0.3 - 0.5 \ eV$$

depending on the calculation chosen.

Also the sensitivity to two-neutrino double-beta ($2\nu\beta\beta$) decay will be improved, essentially by the ratio of normalized backgrounds. Without making any background subtraction, which is in general not very safe, the present Xe TPC has reached a limit of

$$T_{1/2}^{2\nu} > 2.3 \cdot 10^{20} \ yr.$$

The $\overline{\nu}_e e^-$ TPC sensitivity would thus extend up to

$$T_{1/2}^{2\nu} \sim 10^{22} \ yr,$$

well above the half-life of $T_{1/2}^{2\nu} \sim 1 - 3 \cdot 10^{21} \ yr$ expected from the Caltech calculation [77]. This would allow for a stringent test of this calculation, and make the neutrino mass determination safer. Similarly, a sensitive search of double beta decay with Majoron emission [80], [81], [82] could be performed with the $\overline{\nu}_e e^-$ TPC.

Since the drift velocity in Xe gas is about 4 to 5 times slower than in CF_4, and for optimal background, it would be desirable to set up the $\overline{\nu}_e e^-$ TPC in an underground facility for this experiment. At present, 3000 liters of Xe enriched to 62.5 % in ^{136}Xe are available in Western Europe. It seems that it should be possible to get an additional 2000 liters from Ukraina or Russia.

VI.2 Search for Dark Matter

There are several indications, for instance from the dynamics of stars and gas in galaxies, that the universe contains a large amount of dark matter, about 3–10 times more than luminous matter [83]. One good candidate, favored by galaxy formation, is cold dark matter (CDM), made from heavy, say more than a few GeV, non-relativistic weakly interacting particles. Such particles would be gravitationally bound in galaxies,

and would form a non-corotating halo, in which stars would orbit. CDM can, with a small probability, hit a nucleus of normal matter and transfer recoil energy to it. Although small, typically a few keV, the recoil can be measured if the nucleus belongs to the active part of a detector, making direct detection of dark matter possible.

So far, no positive evidence has been found, and the best limits have been obtained with low background Ge detectors operated underground [84], [85]. The threshold energy is around 3 keV, and the background level above that is of order 1 $count \cdot kg \cdot keV \cdot day$. The masses are of order 1 kg. A large portion in the mass versus cross-section plane can be ruled out. For Dirac neutrinos, the cross-section is expected to be relatively large, since it scales essentially with the square of the number of neutrons in the struck nucleus, which interacts coherently. The Ge limits allow essentially to eliminate heavy Dirac neutrinos with standard coupling as the main constituent of the dark matter. Dark matter particles may however have no vector coupling, and only axial coupling, with normal matter. So are, for instance, Majorana neutrinos, or the lightest supersymmetric particle (LSP), a mixture of neutral gauginos and higgsinos, commonly called neutralinos. The LSP is presently the candidate preferred by particle theorists [86], [87]. In that case the cross-section vanishes for spin zero nuclei, and is finite for nuclei with spin, but small since there is no coherence. For Ge, the only isotope with spin is ^{73}Ge with an abundance of 7.7 %. Therefore, experiments with Ge detectors can only constrain in a limited way the parameter space of these particles [88].

Two better candidates are F, which is pure ^{19}F with spin 1/2+, and Xe, containing 26.4 % of ^{129}Xe (1/2+), and 21.1 % of ^{131}Xe (3/2)+. The $\overline{\nu}_e e^-$ TPC, filled with CF_4 at 5 bars, would contain a mass of 15.5 kg of ^{19}F. This is 150 times more mass than in the ^{73}Ge of a classical Ge detector. With 5 bars of Xe, one would have a total mass of 29 kg, of which 13.6 kg would be in ^{129}Xe and ^{131}Xe. The energy threshold in the TPC can be lowered down to 2 to 3 keV. It is not easy at this time to estimate the background just above that threshold. There is a reasonable hope however that, thanks to the anti-Compton and the imaging provided by the TPC, it can be reduced to a level much less than that in a Ge detector. The TPC would then be a powerful tool for a search with presently unknown sensitivity for dark matter particles with axial coupling. With Xe, also a large mass nucleus, the sensitivity would also be very good for particles with vector coupling, and the sensitivity obtained with solid state Ge detectors would be surpassed, and one could look for neutrinos with non-standard coupling [89]. With the large mass, one could look for the 10 % annual modulation of the event rate, due to the change in relative earth-halo velocity, capable of giving a positive signature.

To come back to the LSP, it is not easy to make an exact prediction of what part of the parameter space can be explored, since the number of parameters is large (3, in the simplest scheme, in addition to the mass of the LSP). The correlation between these parameters and the nuclear physics part is strong, and does not follow a simple pattern. Also, the estimates for a given nucleus can vary significantly from author to author [90], [91]. But, according to ref. [87], ^{19}F is an excellent candidate, and the reaction rate in the TPC should be above 0.1 to 1 count per day, presumably the detection threshold, for a large portion of the parameter space. With Xe, one could extend the search to a

different part of the parameter space. In any event, a search with F and Xe would be complementary to planned experiments using enriched ^{73}Ge, or NaI [92].

Clearly, to definitely assess the potentiality of the TPC as a dark matter detector, one needs to know more about the low energy background. We plan to study it, in Bugey, while taking data on $\overline{\nu}e^-$ scattering. If a level low enough is achieved, it would be very tempting to move the TPC underground, where the background conditions are optimal, and look for dark matter particles.

References

[1] B.W. Lee and R.E. Shrock, Phys. Rev. D 16(1977)1444

[2] W. Marciano and A.I. Sanda, Phys. Lett. B 67(1977)303

[3] M.B. Voloshin, Sov. J. Nucl. Phys. 48(1988)

[4] K.S. Babu and R.N. Mohapatra, Phys. Rev. Lett. 63(1989)228

[5] M. Leurer at al., Phys. Lett. B 237(1990)81

[6] R. Barbieri et al., Phys. Lett. B 252(1990)251

[7] S.M. Barr, E.M. Friere and A. Zee, Phys. Rev. Lett. 65(1990)2626

[8] B.K. Pal, Phys. Rev. D 44(1991)2261

[9] P. Vogel and J. Engel, Phys. Rev. D 39(1989)3378

[10] B. Kayser et al., Phys. Rev. D 20(1979)87

[11] K. Lande, talk given at the Neutrino 1990 Conf., Geneva

[12] F. Boehm and P. Vogel, *Physics of Massive Neutrinos*, Cambridge University Press, 1987

[13] T. Totsuka, Proc. Neutrino 1990 Conf., Nucl. Phys. B(Proc. Suppl.) 19(1991)69

[14] M.B. Voloshin, M.I. Vysotskii and L.B. Okun, Sov. Phys. JETP 64(1986)446

[15] C.S. Lim and W.J. Marciano, Phys. Rev. D 37(1988)1368

[16] E.K. Akhmedov, Phys. Lett. B 213(1988)64

[17] K.S. Babu, R.N. Mohapatra and I.Z. Rothstein, Phys. Rev. D 44(1991)2265

[18] Y. Ono and D. Suematsu, Phys. Lett. B 271(1991)165

[19] E. Gates, L. Krauss and M. White, Phys. Rev. D 46(1992)1263

[20] Z.G. Berezhiani et al., Phys. Lett. B 264(1991)381

[21] P.I. Krastsev and A.Yu Smirnov, Z. Phys. C 49(91)675; P.I. Krastsev, *Time Variation of Solar Neutrino Signals and the RSFC hypothesis*, CERN TH 6648/92;

[22] E.Kh. Akhmedov, A. Lanza, S.T. Petcov, preprint SISSA-172/92/EP

[23] Gallex collaboration, P. Anselmann et al., Phys. Lett. B 285(1992)376

[24] Gallex collaboration, P. Anselmann et al., Phys. Lett. B 285(1992)390

[25] J.M. Lattimer and J. Cooperstein, Phys. Rev. Lett. 61(1988)23

[26] R. Barbieri and R.N. Mohapatra, Phys. Rev. Lett. 61(1988)27

[27] D. Notzold, Phys. Rev. D 38(1988)1658

[28] J. Bernstein et al., Phys. Rev. 132(1963)1227

[29] P. Sutherland et al., Phys. Rev. D 13(1976)2700

[30] G. Raffelt, Phys. Rev. Lett. 64(1990)2856

[31] R.C. Allen et al., Phys. Rev. Lett. 55(1985)2401

[32] D.A. Krakauer at al., submitted to Phys. Lett. B

[33] G. Zacek et al., Phys. Rev. D 34(1986)2621

[34] F. Reines, H.S. Gurr and H.W. Sobel, Phys. Rev. Lett. 37(1976)315

[35] F.T. Avignone, Phys. Rev. D 2(1970)2609

[36] D. Geiregat et al., Phys. Lett. B 232(1989)539

[37] I.I. Gurevitch et al., preprint, I.V. Kurtchatov Institute of Atomic Energy, 123182 Moscow, Russia, 1991; G.S. Vidyakin et al., JETP Lett. 49(1989)740 Zürich collaboration, Letter of intent, 1991

[38] D.H.Koang, Proc. XVIth rencontres de Moriond, QCD and Lepton physics, Editions Frontières,(1981)187 and J. Collot, Proc. XXIIIrd rencontres de Moriond, 5th Force and Neutrino Physics, Editions Frontières, 1988

[39] J.F. Cavaignac et al. Phys. Lett. 148B (1984)387

[40] H. De Kerret in Proc. of Moriond Workshops (1988)

[41] E. Kajfasz in Proc. of Moriond Workshops April(1992)

[42] Gran-Sasso, Grenoble, Münster, Neuchâtel, Padova, letter of intent

[43] H. Wong et al., Phys. Rev. Lett. 67(1991)1218; H. Wong, PhD thesis, Caltech, 1990; M.Z. Iqbal et al., Nucl. Inst. Meth. A 259(1987)459

[44] A. Peisert and F. Sauli, CERN yellow report 84-08, 1984; L. G. Christophorou et al., Nucl. Inst. and Meth. 163(1979)141

[45] B. Schmidt and S. Polenz, Nucl. Inst. Meth. A 273(1988)488; K. Martens, Diplomarbeit, Universität Heidelberg, 1989

[46] C. Broggini et al., Nucl. Inst. and Meth. A 311(1992)319

[47] P. Vogel et al., Phys. Rev. C 24(1981)1543

[48] H.V. Klapdor et al., Phys. Rev. Lett. 48(1982)127; Phys. Lett. B 112(1982)22

[49] F. v. Feilitzsch et al., Phys. Lett. 118B(1982)162

[50] K. Schreckenbach et al., Phys. Lett. 160B(1985)325

[51] K. Schreckenbach et al., in Weak and Electromagnetic Interactions in Nuclei, Proc. Int. Symp., Heidelberg 1–5 July 1986, Springer, p.759

[52] A. Hoummadda These de doctorat, Univ. de Grenoble(1984)

[53] M.F. James, J. Nucl. Energy 23(1969)517; J.M. Paratte, Swiss Federal Institute for Reactor Research, Report No. TM-45-81-19 (unpublished)

[54] K. Schreckenbach ILL Grenoble, technical report 84SC26T

[55] C. Broggini et al., NIM A311(1992)319

[56] R. Arnold et al., The NEMO2 Detector, Technical Note NEMO 9/92, LAL Orsay

[57] M. Avenier et al., rapport interne ISN Grenoble (1992)

[58] F. Boehm et al., Caltech Report CALT-63-630 (Nuclear Physics)

[59] BOREXINO proposal, August 1991

[60] C. Arpesella, private communication

[61] E.D. Hallman, SNO collaboration, Low Background Research for the Sudbury Neutrino Observatory, contributed paper to the XV International Conference on Neutrino Physics and Astrophysics, 7–12 June 1992, Granada, Spain

[62] G. Heusser and M. Wojcik, Radon Suppression in Low Level Counting, Proc., ICRM Meeting on Low Level Radioactivity Measurements and Alpha Particle Spectrometry, Monaco, June 4–6 1991, to appear in Appl. Rad. and Isot.

[63] A. Alessandrello et al., NIM B 61(1991)106

[64] J. D. Fassett and W.R.Kelly., NIM B 69(1992)503

[65] R.Brun et al.,GEANT-CERN Program Library

[66] G.Bagieu, GAMTRACK, ISN-Grenoble Int. Rep.1992

[67] Cocconi et Tongiori,Phys. ReV. 84,29 (1951)

[68] Suzuki et al. Phys. Rev. C 35 (1987) 2212

[69] N.C.Mukhopadhyay, Phys. Rep. C 30 (1977) 1

[70] S.Charalamalus, Nucl.P hys.A 166 ,145 (1971)

[71] M.Aglietta et al., Il Nuovo Cimento 12C (1989) 467

[72] C.Arpesella, Nucl. Phys. B (proc.suppl)28A(1992) 420

[73] cited in Proposal for Large Cerenkov Detector, Los Alamos,1988. LA-11300-P

[74] A. Hoummada, Rapport ISN 92-85(1992)

[75] W.U.Schroeder et al, Zeit. für Phys. 268(1974)57–64

[76] A. Balysh et al., Phys. Lett. B 283(1992)32

[77] J. Engel, P. Vogel and M.R. Zirnbauer, Phys. Rev. C 37(1988)731; see also ref. [43]

[78] K. Muto, E. Bender, and H. V. Klapdor, Zeit. für Phys. A 334(1989)187

[79] J. Suhonen, S.B. Khadkikar and A. Faessler, Nucl. Phys. A 535(1991)509

[80] H. Georgi, S. Glashow, and S. Nussinov, Nucl. Phys. B 193(1981)297

[81] M.K. Moe et al., UCI-NEUTRINO 92-1, preprint

[82] Z.G. Berezhiani, A. Yu. Smirnov and J.W.F. Valle, FTUV92-20 preprint, 1992

[83] J. Primack, D. Seckel and B. Sadoulet, Annu. Rev. Part. Sci. 38(1988)751

[84] D. Reusser at al., Phys. Lett. B 255(1991)143

[85] D.O. Caldwell et al., Phys. Lett. 61(1988)510

[86] J. Ellis and R.A. Flores, Nucl. Phys. B 307(1988)883

[87] J. Ellis and R.A. Flores, Phys. Lett. B 263(1991)259

[88] G.B. Gelmini, P. Gondolo and P. Roulet, Nucl. Phys. B 351(1991)623

[89] J. Ellis et al., Phys. Lett. B 245(1990)251

[90] J. Engel and P. Vogel, Phys. Rev. D 40(1989)3132

[91] J. Engel, Phys. Lett. B 264(1991)114

[92] WIMPS search with low activity NAI crystals: preliminary results, Beijing-Roma-Saclay collaboration, C. Bacci et al., to appear in Phys.lett. B, LNGS 92/36, July 1992

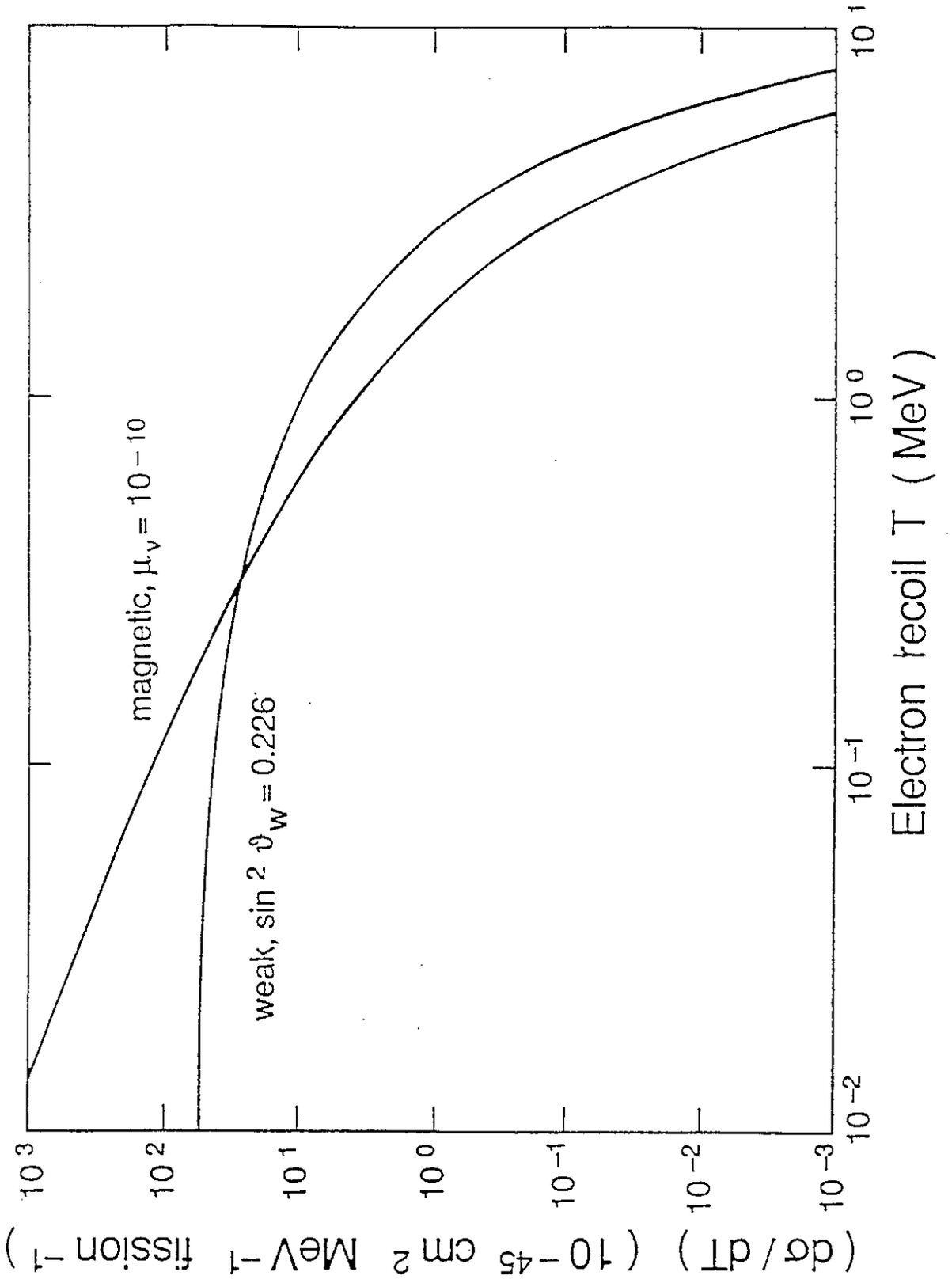

Figure 1: Contributions to the expected cross-section for $\bar{\nu}_e e^- \to \bar{\nu}_e e^-$ scattering averaged over the reactor $\bar{\nu}_e$ spectrum. The contribution from weak interaction alone (first line of eq. 3) and from a magnetic moment $\mu_\nu = 10^{-10}$ alone (second line) are shown separately [9].

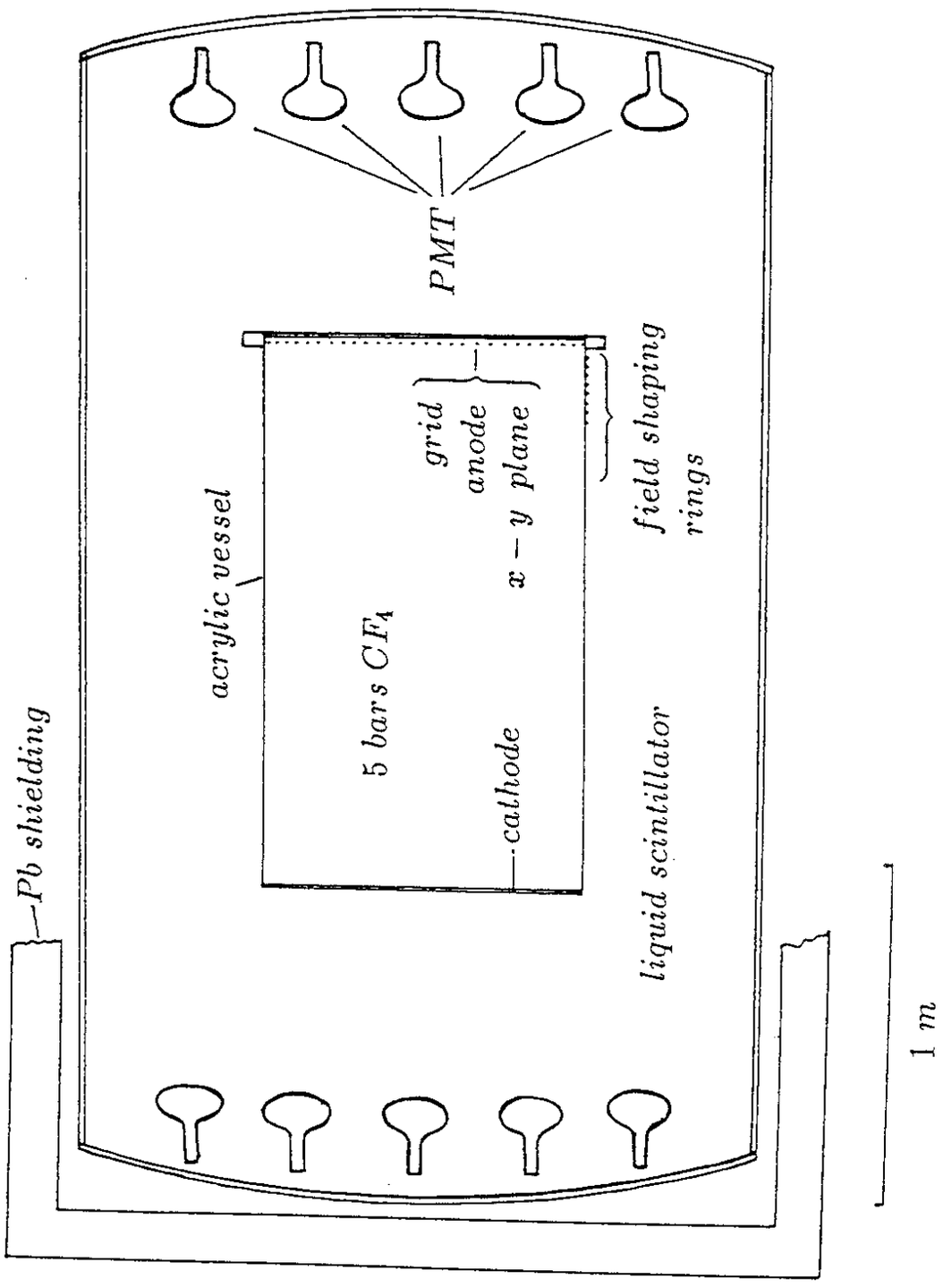

Figure 2: General layout of the detector.

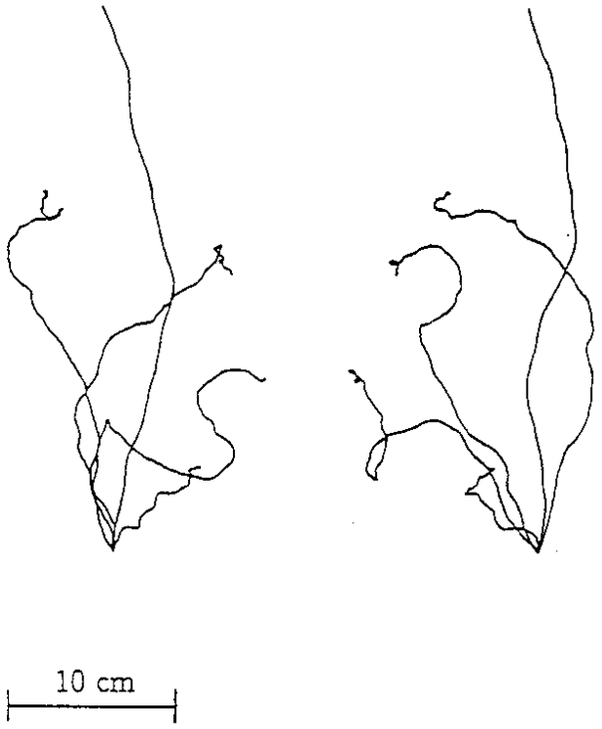

Figure 3: Simulated electron tracks ($T > 0.5\ MeV$) in CF_4 at 5 *bars* from $\overline{\nu}_e e^-$ at a reactor. The neutrinos come along the z axis, the $x-z$ and $y-z$ projections are shown.

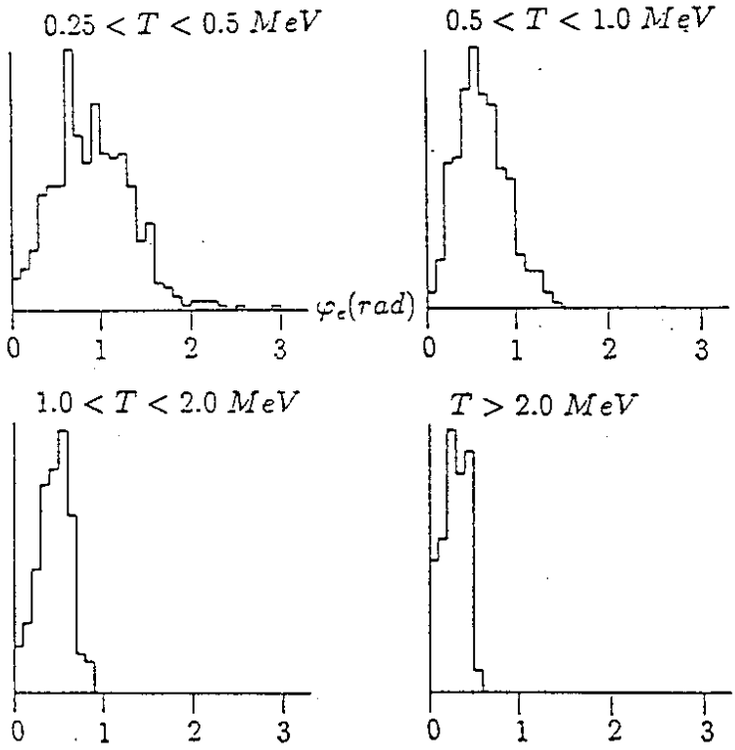

Figure 4: Simulated angular distribution of the recoil electron determined from the first 2 *cm* of track in CF_4 at 5 *bar*.

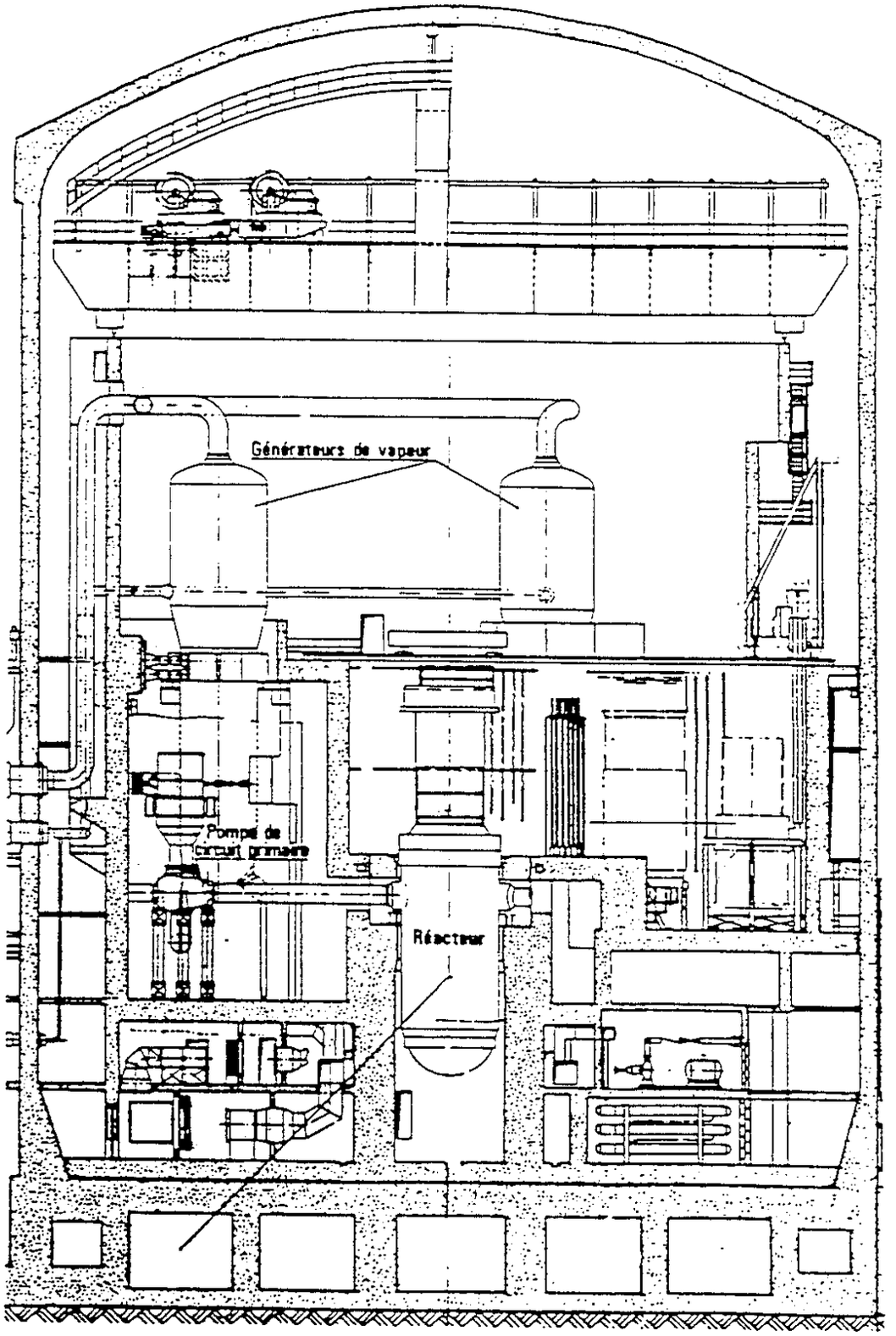

Figure 5: The Bugey Reactor Building

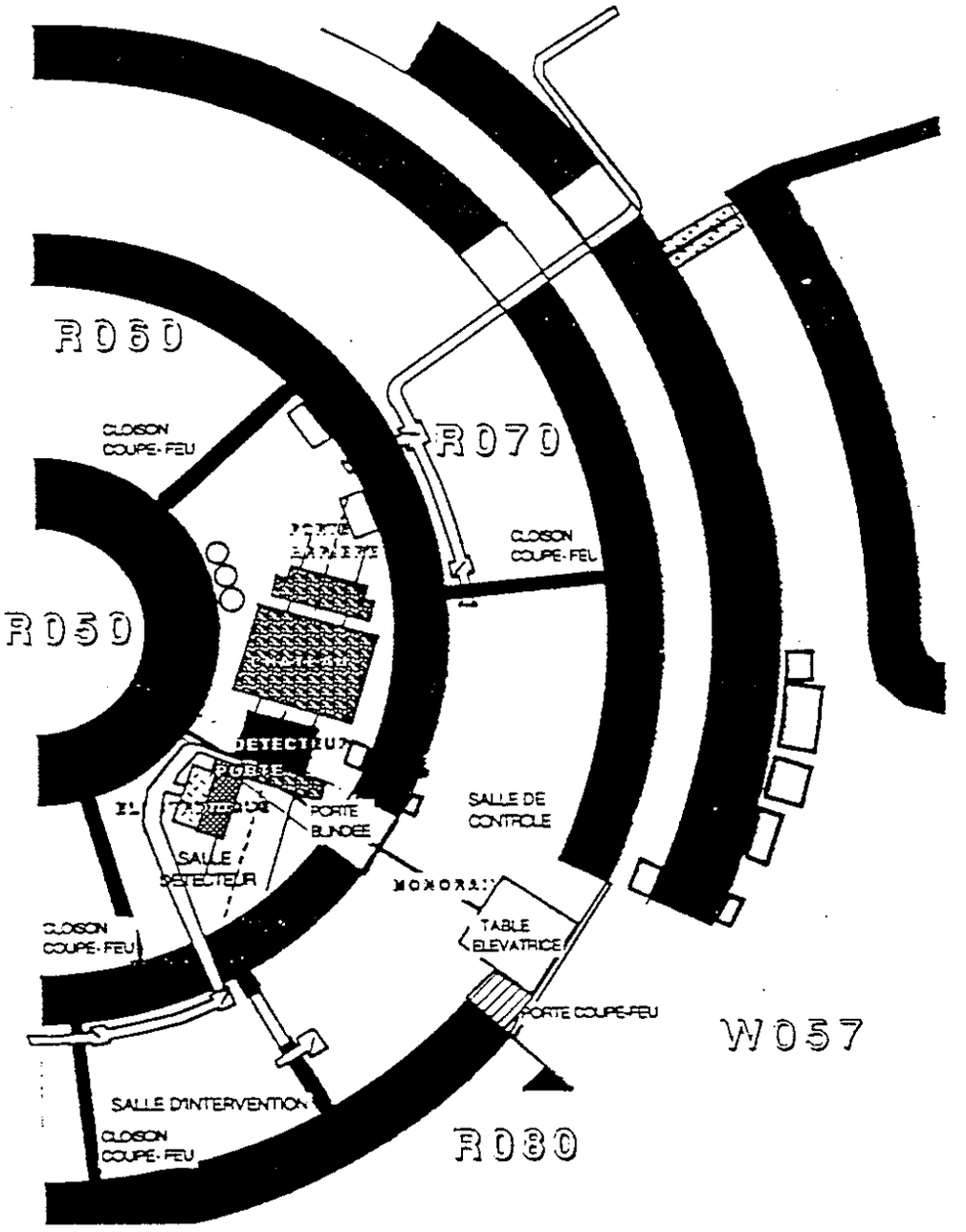

Figure 6: The experimental area in the basement of the Bugey reactor

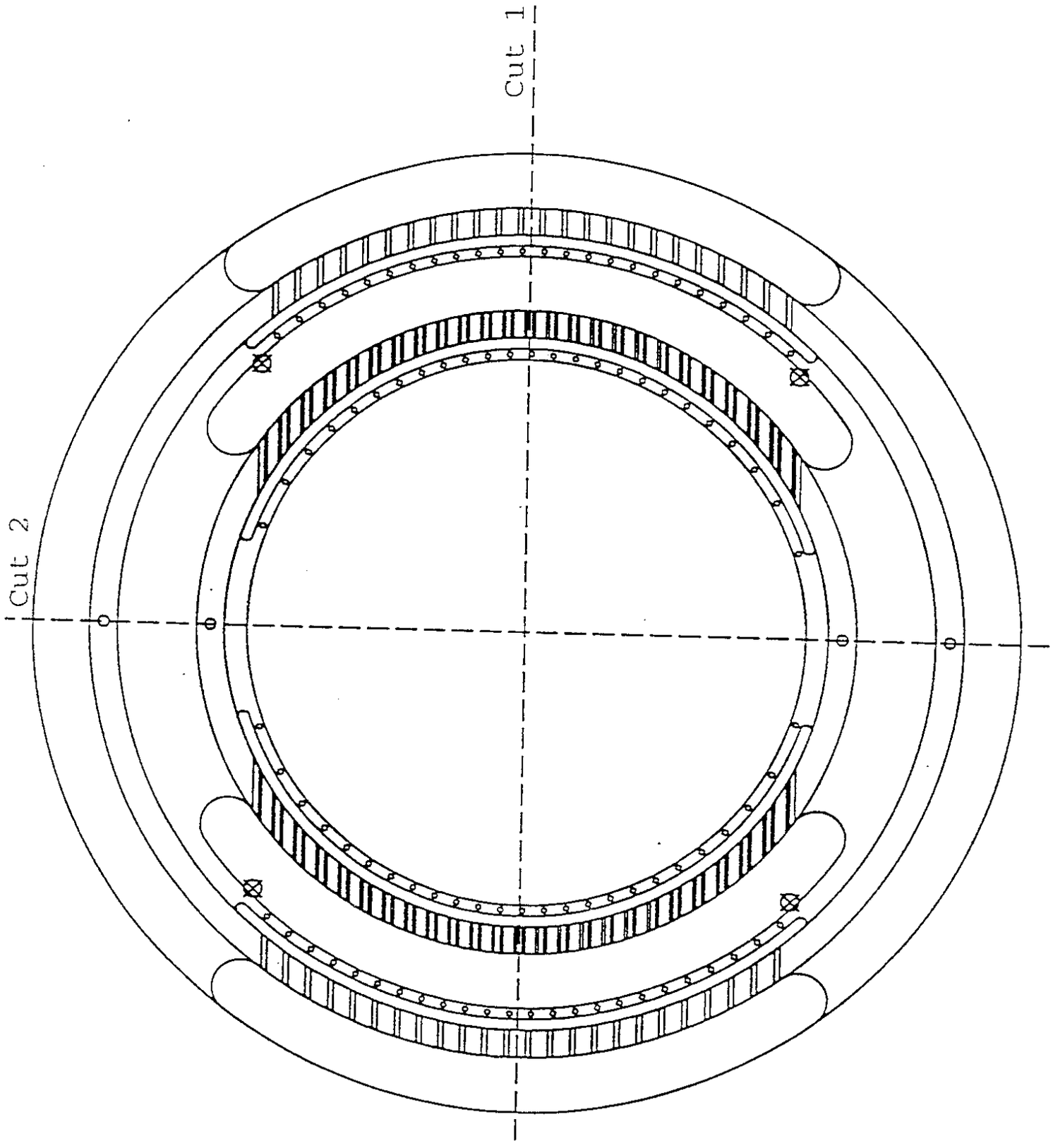

Figure 7: The prototype anode plane with crimped wires. The body of the frame is made from low activity acrylic. The crimps are fixed to Cu pieces embedded in the acrylic. The final anode plane will be similar, except for the overall diameter which will be 90 cm (internal), and for a reinforcement ring cast in the acrylic and made from Cu or carbon fiber.

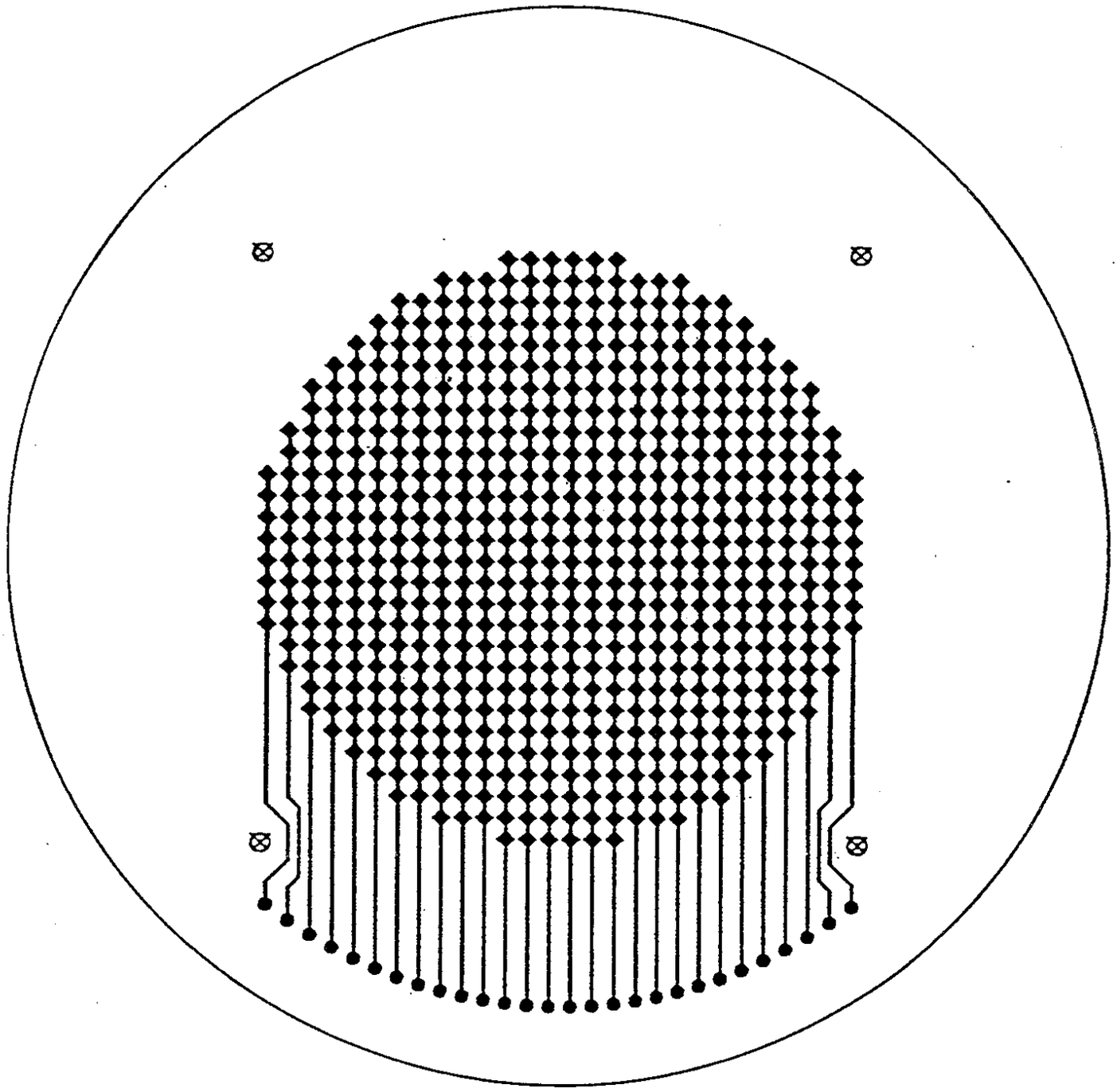

Figure 8: The prototype $x-y$ plane. The x side alone is shown, as well as the superimposed x and y. The stripes are evaporated on a 100 μm thick mylar foil.

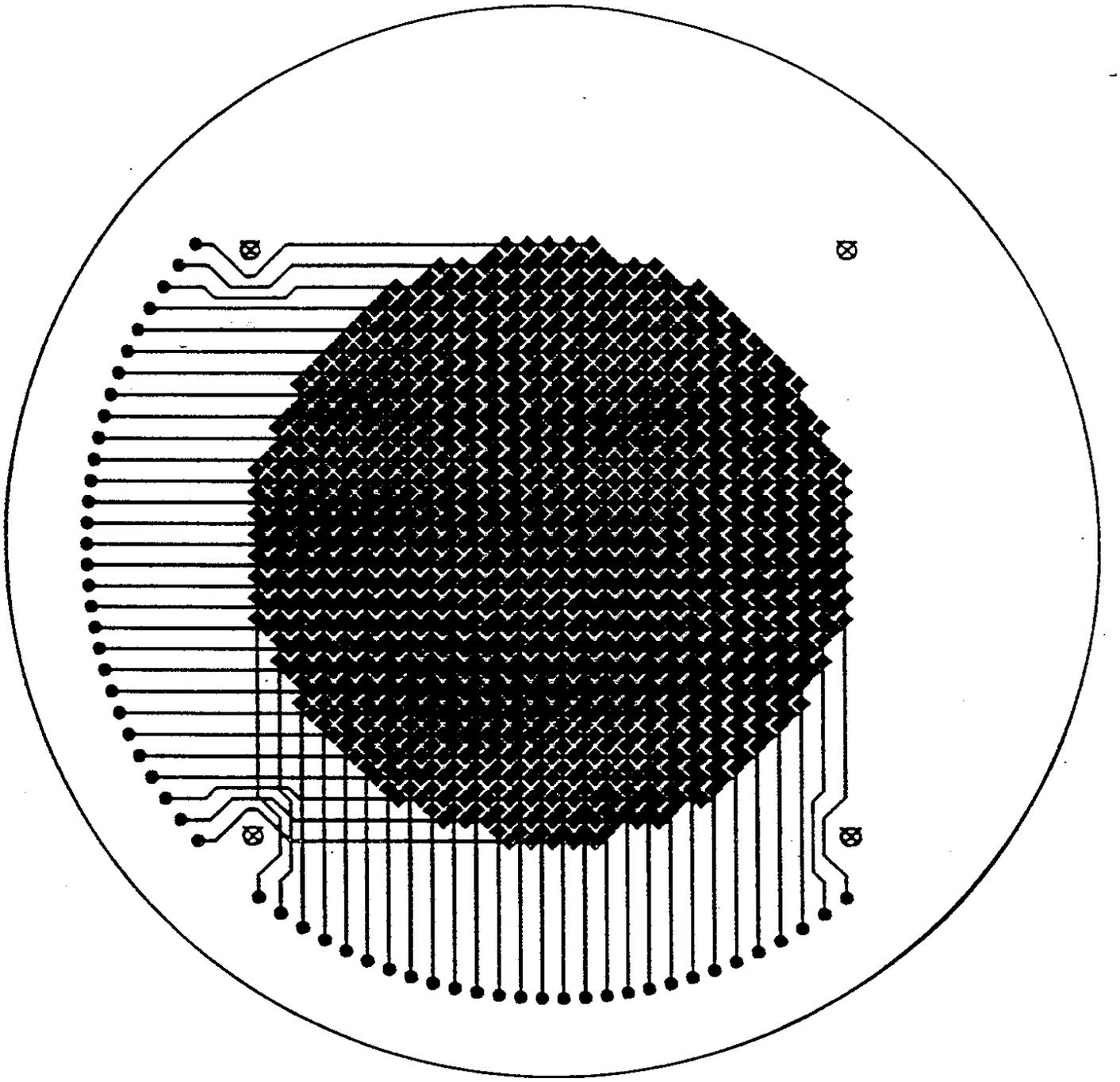

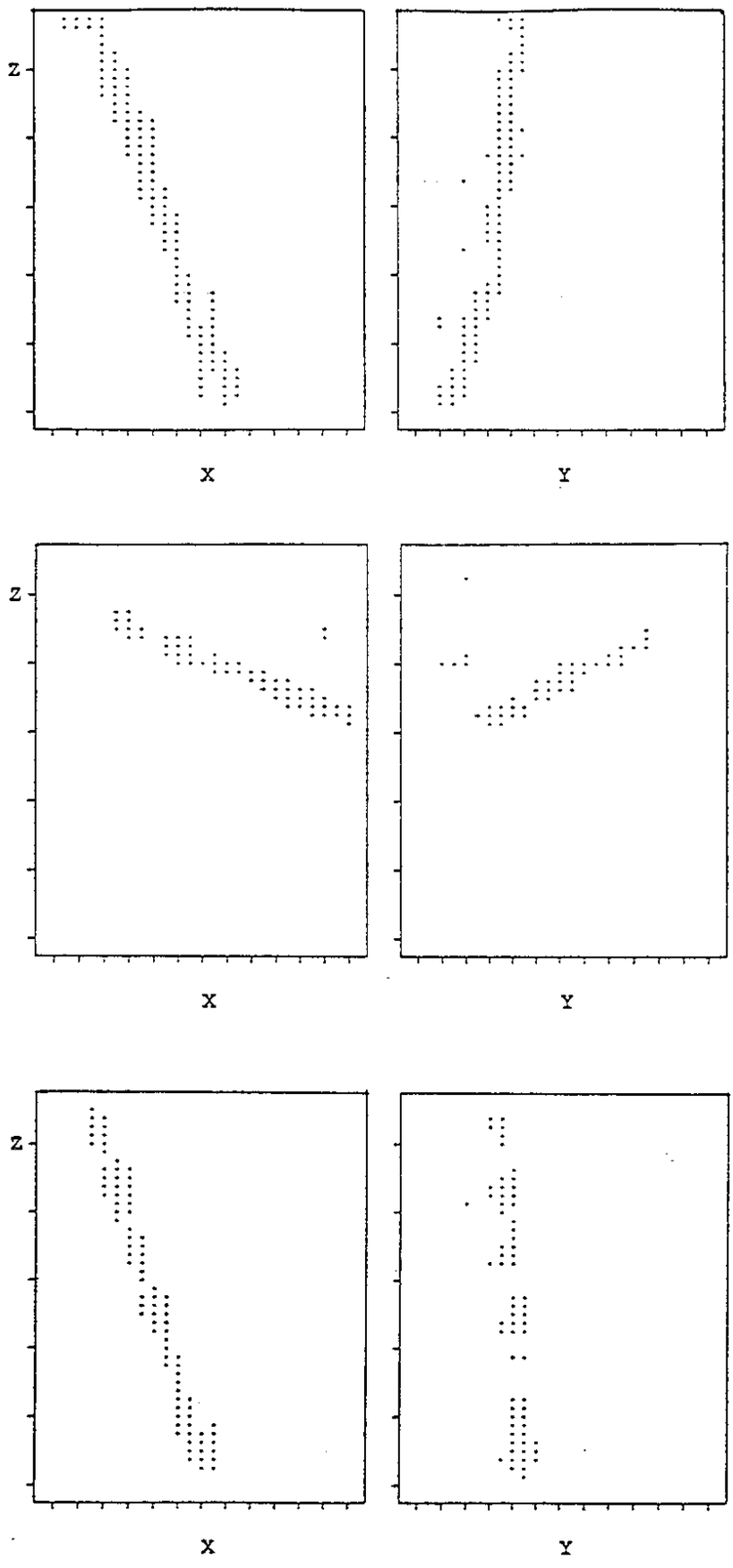

Figure 9: Example of muon tracks observed in the mini-TPC with 5 bars of CF_4. The drift field is 500 $V \cdot cm^{-1}$. The vertical scale is 4 cm per unit. The horizontal scale is 0.5 cm per unit.

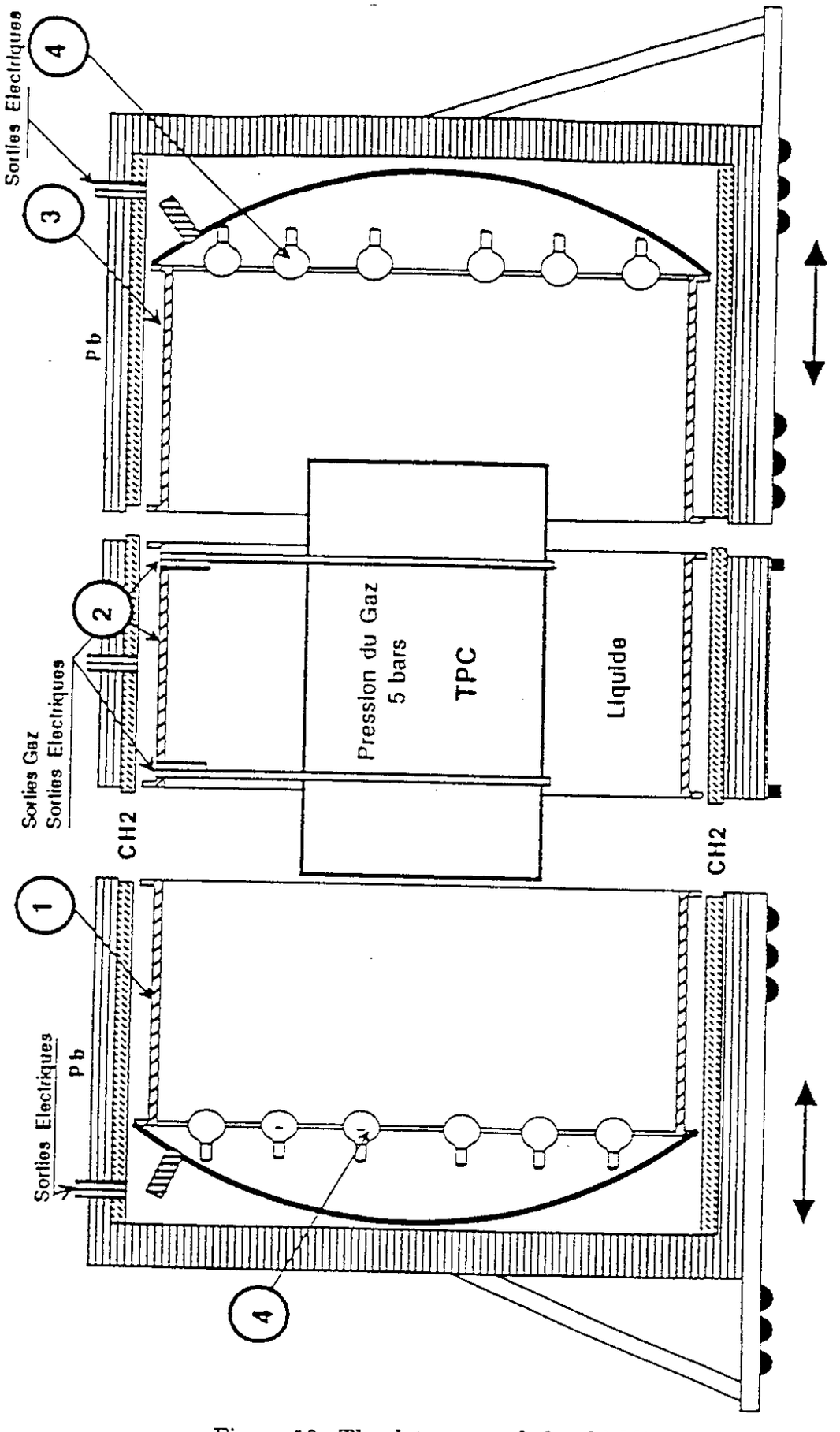

Figure 10: The detector and the shielding.

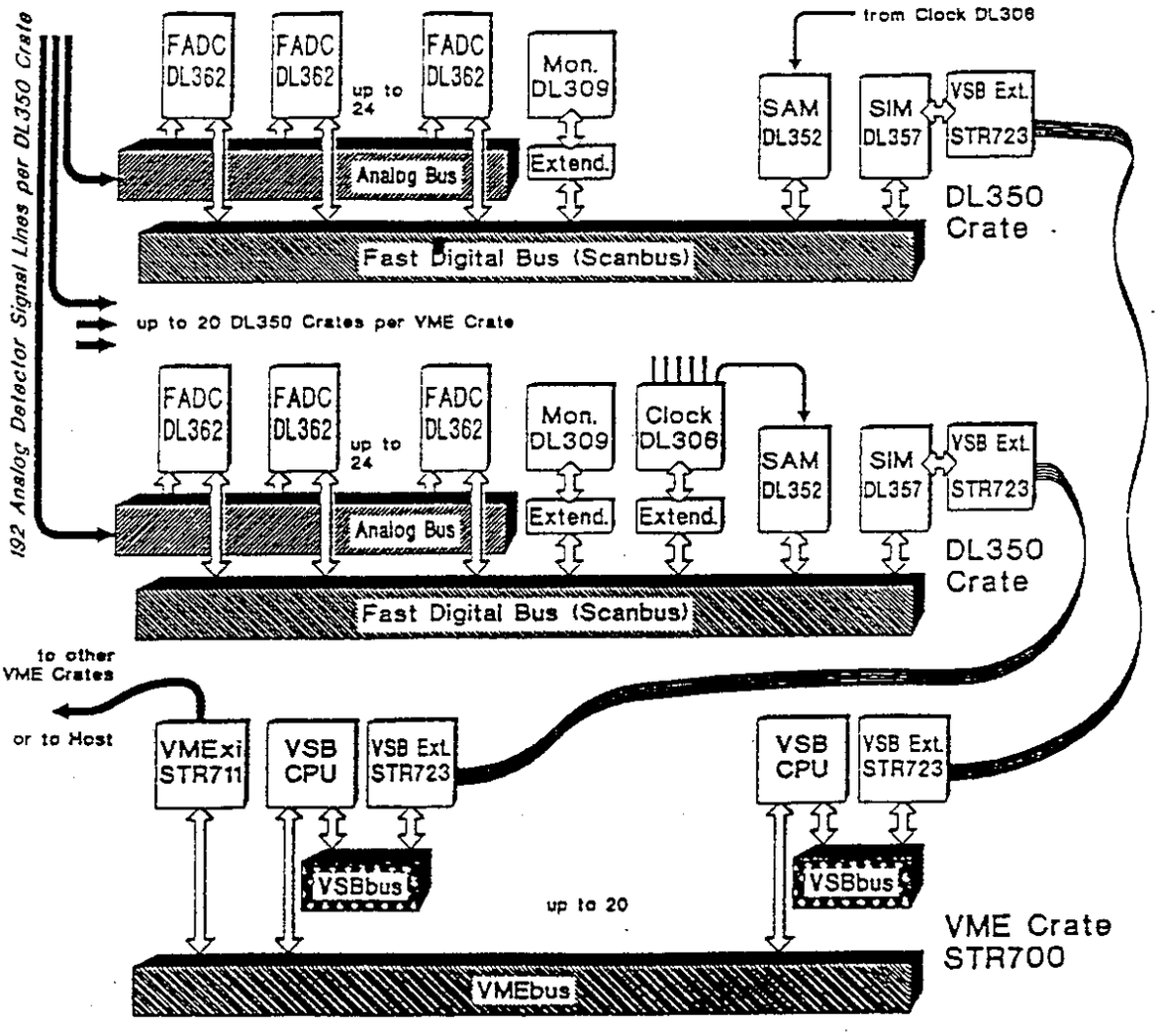

Figure 11: The DL350 FADC System Diagram (see text).

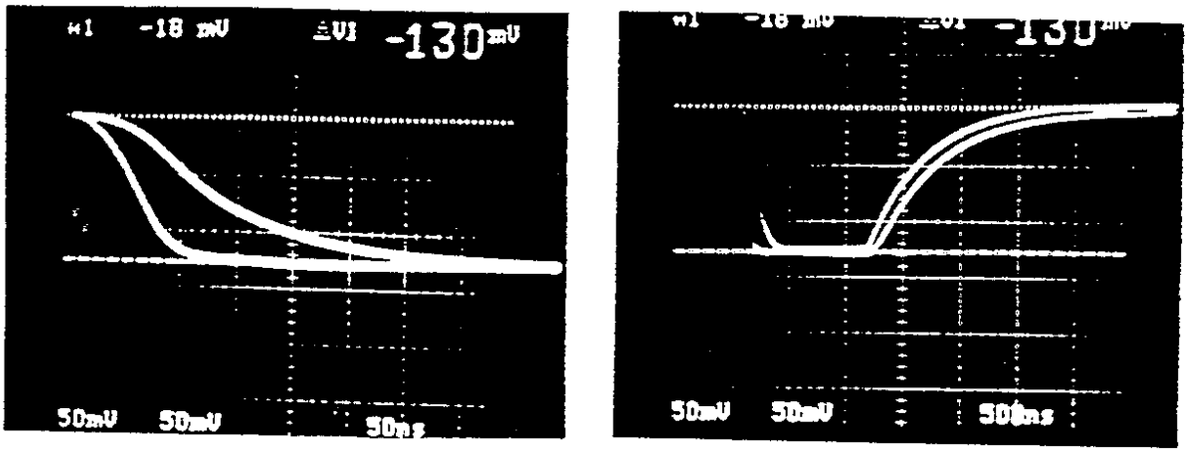

Figure 12: Analog test signals given by the external pulser with and without the preamplifier. Both amplitudes are normalized. The signal defined by the preamplifier has the longer rise time of $\sim$300 ns. Only the first 400 ns (50 ns/div) are shown.

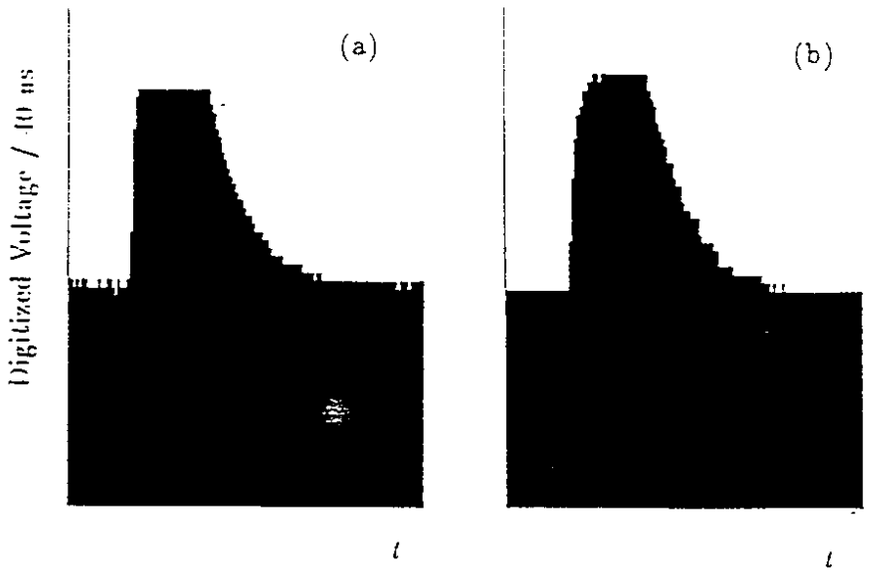

Figure 13: Digitized signal before (a) and after preamplification (b). The signal amplitude (vertical axis) is shown as a function of time (horizontal axis). The sampling frequency is 25 MHz which corresponds to 40 ns per bin. Only the first 128 bins among 1024 are shown.